Research Article

PECTATE LYASE LIKE12 patterns the guard cell wall to coordinate turgor pressure and wall mechanics for stomatal function in *Arabidopsis thaliana*

Yintong Chen[a], Wenlong Li[b], Joseph A. Turner[b], and Charles T. Anderson[a*]

[a] Department of Biology, The Pennsylvania State University, University Park, PA 16802 USA
[b] Department of Mechanical and Materials Engineering, University of Nebraska-Lincoln, Lincoln, Nebraska 68588 USA
*Corresponding author: cta3@psu.edu

Short Title: Pectin influences stomatal biomechanics

One sentence summary: A pectate lyase like gene influences wall mechanics and cell pressurization in guard cells, contribute to stomatal dynamics and plant growth.

The author responsible for distribution of materials integral to the findings in this article in accordance with the policy described in the Instruction for Authors (www.plantcell,org) is: Charles T. Anderson (cta3@psu.edu)

Abstract

Plant cell deformations are driven by cell pressurization and mechanical constraints imposed by the nanoscale architecture of the cell wall, but how these factors are controlled at the genetic and molecular levels to achieve different types of cell deformation is unclear. Here, we use stomatal guard cells to investigate the influences of wall mechanics and turgor pressure on cell deformation, and demonstrate that expression of a pectin modifying gene, *PECTATE LYASE LIKE12* (*PLL12*), is required for normal stomatal dynamics in Arabidopsis thaliana. Using nanoindentation and finite element modeling to simultaneously measure wall modulus and turgor pressure, we find that both values undergo dynamic changes during induced stomatal opening and closure. *PLL12* is required for guard cells to maintain normal wall modulus and turgor pressure during stomatal responses to light and to tune levels of calcium cross-linked pectin in guard cell walls. Guard cell-specific knockdown of *PLL12* causes defects in stomatal responses and reduced leaf growth that correlates with lower cell proliferation but normal cell expansion. Together, these results force us to revise our view of how wall-modifying genes modulate wall mechanics and cell pressurization to accomplish the dynamic cellular deformations that underlie stomatal function and tissue growth in plants.

Introduction

Stomatal dynamics regulate CO_2 and water flux in plants to enable photosynthesis and transpiration. Inflation or deflation of guard cells results in the opening or closure of stomata, respectively. Guard cell deformations are thought to be driven by turgor pressure changes and constrained by the cell wall (Aylor et al., 1973; DeMichele and Sharpe, 1973). However, the influence of cell wall architecture and metabolism on cell biomechanics and pressurization during deformation is poorly understood. Improving our understanding of stomatal biomechanics and how cell wall-related genes impinge on those biomechanics have the potential to open new opportunities to engineer stomatal activity for optimal plant growth under challenging conditions such as drought.

The primary wall of growing plant cells is a composite material with cellulose microfibrils embedded in a pectin-containing matrix (Cosgrove, 2018). Pectins appear to be particularly important for stomatal function, since they are present in guard cells of plant species that contain very little overall pectin (Jones et al., 2005). Stomatal responses to environmental stimuli are influenced by pectin methylesterases (PMEs) and polygalacturonases (PGs), which respectively modulate the methylation state of pectic homogalacturonan (HG) and hydrolyze demethylated HG (pectate) (Amsbury et al., 2016; Huang et al., 2017; Jones et al., 2005; Jones et al., 2003; Rui et al., 2017; Yi et al., 2018). Pectate lyases (PLs) cleave pectate by β-elimination, but their functions in stomatal dynamics have not been studied. We hypothesize that PLs contribute to stomatal dynamics differently than PGs because despite the fact that both classes of enzymes cleave the HG backbone, they have differing mechanisms of action and have independent evolutionary histories (McCarthy et al., 2014).

Because pectins are negatively charged and form hydrated gels and thus have tunable biochemical and biomechanical properties, pectin modification is thought to facilitate cell expansion (Xiao et al., 2014) or cell separation (Babu and Bayer, 2014) in different developmental contexts. Pectate can also be crosslinked by calcium, which increases the elastic modulus of pectin gels *in vitro* (Ström et al., 2007). However, in plant cell walls, both higher (Daher et al., 2018) and lower (Peaucelle et al., 2011) wall stiffness

are associated with more calcium crosslinking, and the functions of pectin and its metabolism, configurations, and crosslinking in plant cell deformation remain unclear.

In the context of stomatal dynamics, mathematical models (Woolfenden et al., 2017; Yi et al., 2018) and Atomic Force Microscopy (AFM) of plasmolyzed guard cells (Carter et al., 2017) have begun to reveal the contributions of HG to the mechanics of guard cell walls, but exactly how HG and other wall components, plus their interactions, influence the extent and kinetics of guard cell deformation during stomatal responses to stimuli are not known. Because pectins function in wall integrity signaling (Feng et al., 2018; Kohorn et al., 2009), pectinases might act not only directly on cell wall mechanics but also via intracellular signaling pathways to influence cell pressurization, which ultimately drives plant cell expansion (Ortega, 1985). Although a pressure probe can be used to measure turgor pressure in species with large guard cells (Franks et al., 1995), turgor pressure has been more difficult to quantify in organisms with smaller guard cells like *Arabidopsis thaliana*, which has a multitude of genetic resources for investigating the cell wall. Although AFM has been used for dynamic measurement of cell wall mechanics (Milani et al., 2014; Yakubov et al., 2016) and for measurement of turgor pressure (Beauzamy et al., 2015), simultaneous tracking of wall modulus and turgor pressure during stomatal movements requires a non-disruptive method that is beyond the capabilities of the pressure probe or AFM methods in isolation. Recently, nanoindentation has been combined with Finite Element Modeling (FEM) to simultaneously estimate wall mechanics and turgor pressure values in living, pressurized pavement cells of *Arabidopsis* (Forouzesh et al., 2013; Routier-Kierzkowska et al., 2012; Li et al., 2021; Weber et al., 2015), opening the possibility to quantify time-resolved mechanical dynamics for *Arabidopsis* guard cells in motion.

Here, we integrate biomechanics, genetic, and physiological approaches to study the influence of pectin on guard cell walls and stomatal dynamics. Our nanoindentation-FEM analyses reveal unexpected dynamic changes in both wall modulus and turgor pressure during stomatal responses to changing light conditions in wild type plants. We demonstrate that a pectate lyase in *Arabidopsis thaliana*, *PECTATE LYASE LIKE12*

(*PLL12*), is required for normal stomatal function, and use nanoindentation-FEM to show that *PLL12* is required to build guard cells with normal biomechanical properties including directional wall modulus and turgor pressure, likely due to its influence on HG abundance and crosslinking in the guard cell wall. The phenotypes of guard cell-specific knockdown lines for *PLL12* indicate that the guard cell-specific functions of this gene are required for cell proliferation and plant growth.

Results

PECTATE LYASE LIKE12 (*PLL12*) Encodes a Putative Pectate Lyase and is Widely Expressed in *Arabidopsis* Plants

To investigate the function of pectate lyase in stomatal function, we mined *Arabidopsis* transcriptome data (Hachez et al., 2011) gathered after the induced expression of FAMA, a transcription factor that drives stomatal differentiation (Ohashi-Ito and Bergmann, 2006). *PECTATE LYASE LIKE12* (*PLL12*) expression is upregulated 48 h after *FAMA* induction (Hachez et al., 2011), suggesting a role in guard cell development and function. Both splice variants encoded by *PLL12* have a Pectate lyase C (PelC) domain and a signal peptide; for transgenic analyses, we used splice variant 1 (Supplemental Figure 1). PLL12 shows high sequence similarity with PLs from multiple plant species and contains conserved residues involved in Ca^{2+} binding, substrate binding, and catalytic activity (Scavetta et al., 1999; Yoder and Jurnak, 1995) (Supplemental Figure 1).

To analyze *PLL12* expression patterns, we transformed a construct containing the 2 kb upstream of the *PLL12* start codon fused to the β-glucuronidase (GUS) gene into *Arabidopsis thaliana* plants of the Columbia-0 (Col) ecotype. GUS activity varied across three independent transformant lines (Supplemental Figure 2), as previously reported (Sun and van Nocker, 2010). Nevertheless, GUS activity was commonly higher in older rosette leaves than in younger leaves (Supplemental Figure 2A). In young seedlings, roots and cotyledons showed GUS activity (Supplemental Figure 2B). In the leaf epidermis, GUS activity was detected in both guard cells and surrounding pavement

cells (Supplemental Figure 2C). These data and previous RT-PCR results (Palusa et al., 2007; Sun and van Nocker, 2010) demonstrate that *PLL12* is widely expressed in roots, leaves, stems, and inflorescences of *Arabidopsis.*

To analyze *PLL12* function, we isolated a T-DNA knockout mutant that we named *pll12-1* (Supplemental Figure 2D). No *PLL12* RT-PCR product was detected in this mutant, suggesting that it is a null mutation (Supplemental Figure 2D). Complementation lines (*PLL12comp*) were generated by transforming a construct containing a *PLL12* promoter::*PLL12* CDS fusion into the *pll12-1* mutant background. RT-PCR showed restored *PLL12* expression in three independent transformant lines (Supplemental Figure 2E), and *PLL12comp-1* was named *PLL12comp* and used for further analyses. A *PLL12* overexpression line was generated by transforming a construct containing a *35S pro::PLL12 CDS* fragment into the Col background, and given similarly elevated levels of *PLL12* expression in three independent transformant lines (Supplemental Figure 2E), *PLL12OE-1* was chosen for further analysis and named *PLL12OE*.

Given the broad expression of *PLL12*, we also constructed guard-cell-specific knockdown lines for this gene. Three different sets of transgenic lines were generated by transforming Col plants with constructs containing a guard-cell-specific promoter, pGC1 (Yang et al., 2008), fused with artificial microRNA (amiRNA) sequences targeting one of three different sites in *PLL12* (Supplemental Figure 2G)*,* and were designated *PLL12kd1 to 3.* As controls, *GFPkd1 to 3* transgenic plants targeting GFP, which is not present in *Arabidopsis*, were constructed.

Expression levels of *PLL12* in Col and transgenic plants were examined using qPCR (Supplemental Figure 2F). Given the age-dependent expression of *PLL12* in leaves (Supplemental Figure 2A), only leaves 5-8 from 21-day-old rosettes were used for qPCR and subsequent assays (Supplemental Figure 2F). Using a ($\log_2$) difference of two as a cutoff, *pll12-1* and all *PLL12kd* leaves had lower *PLL12* transcript levels, *PLL12OE* had higher transcript levels, and *GFPkd* lines had transcript levels similar to Col controls (Supplemental Figure 2F). *PLL12comp* leaves had significantly higher

PLL12 expression levels than Col (Supplemental Figure 2F). Comparing *PLL12kd* to *GFPkd* lines, *PLL12* transcript levels in whole leaves of *PLL12kd2* and *3* were significantly lower than *GFPkd1* and *3* but not lower than *GFPkd2*, and *PLL12* expression in *PLL12kd1* leaves was not statistically different from any *GFPkd* line (Supplemental Figure 2F), indicating more efficient silencing of *PLL12* transcripts in guard cells of *PLL12kd2* and *3* plants than in *PLL12kd1* plants.

PLL12 **Functions in Stomatal Dynamics**

To determine the role of *PLL12* in stomatal function, we assayed stomatal responses to various stimuli in plants of the genotypes described above. The hormone abscisic acid (ABA) or darkness were applied to excised leaves to induce stomatal closure; Fusicoccin (FC), a proton pump activator, or light were used to induce stomatal opening. Every 30 min after treatment, a leaf epidermis was peeled and imaged to track stomatal dynamics for each genotype. In addition to stomatal pore area, pore area:stomatal complex area ratios were calculated for each stomatal complex to quantify the degree of stomatal opening/closing in a way that accounts for variation in stomatal complex size across different genotypes (see below).

In *pll12-1* knockout leaves, stomata responded more slowly to closure and opening stimuli than Col stomata (Figure 1 and Supplemental Figure 3A-F). *pll12-1* stomata also closed further than Col stomata in response to ABA or darkness (Figure 1A and Supplemental Figure 3A, 3C, 3E), and did not open as widely as Col stomata after FC or light induction (Figure 1C and Supplemental Figure 3B, 3D, 3F). *PLL12OE* stomata closed slightly more slowly in response to ABA or dark than Col stomata (Figure 1A-D and Supplemental Figure 3A, 3C ,3E). In opening assays, although *PLL12OE* stomata were slightly less responsive to FC than Col stomata, they opened as fast as Col stomata in response to light, and can open to the same degree as Col stomata (Figure 1C and Supplemental Figure 3B, 3D, 3F). Pore areas in *PLL12OE* stomata were similar to Col at the beginning of FC or light treatment experiments, indicating that *PLL12OE* stomata can close to the same degree as Col stomata (Figure 1C and Supplemental Figure 3B, 3D, 3F). Together, these data suggest that loss of *PLL12* results in stiffer

and/or less readily pressurized guard cells that cannot respond efficiently to environmental stimuli, whereas overexpression of *PLL12* results in guard cells that are as deformable as Col cells, but contract more slowly in response to closure stimuli, implying a defect in the kinetics of wall contractibility and/or guard cell depressurization.

Although we observed altered stomatal dynamics in *pll12-1* plants, the broad expression of *PLL12* (Supplemental Figure 2A-C) raises uncertainty as to whether *PLL12* regulates stomatal function directly via its expression in guard cells. To address this uncertainty, stomatal responses to ABA and FC were measured in *PLL12kd* lines where *PLL12* expression was specifically knocked down in guard cells, as well as in *GFPkd* controls. In these experiments, although *PLL12kd* guard cells did not differ in size from controls (see below), *PLL12kd* stomata showed defective responses to some stimuli: for example, *PLL12kd2* stomata closed and opened more slowly in response to ABA or FC, respectively, than *GFPkd2* stomata (Figure 1E-H). Stomatal pore widths after 2.5 h ABA or FC treatment were measured for all three *PLL12kd* lines, and abnormal stomatal responses were seen in *PLL2kd2* and *PLL12kd3* plants (Supplemental Figure 3I-L), but not in *PLL12kd1* plants (Supplemental Figure 3G-H), which did not show as extensive a reduction in *PLL12* transcript levels (Supplemental Figure 2F). Measurements made 2.5 h after FC treatment and at the beginning of ABA treatments (after leaves were pre-incubated in light for 2.5 h) indicated that *PLL12kd* stomata are unable to open as widely as controls (Figure 1E-H Supplemental Figure 3I-L). In most cases after induction of stomatal closure, *PLL12kd* stomata were closed to a higher degree than *GFPkd* controls (Figure 1G time 0, Supplemental Figure 3I, 3J, 3L), although in other experiments measuring stomatal responses to ABA, *PLL12kd* stomata ultimately closed to a similar degree as *GFPkd* stomata (Figure 1E, Supplemental Figure 3K). Together, these data support a specific function of *PLL12* in guard cells in facilitating normal stomatal dynamics.

***PLL12* Balances Turgor Pressure and Wall Mechanics in Guard Cells**

After establishing that *PLL12* is required for normal stomatal dynamics, we next investigated the underlying physical mechanism(s) by which *PLL12* affects guard cell

behavior. Previous studies of plant cell mechanics propose that cell wall modifications alter wall mechanics, which in combination with water uptake and cell pressurization determine the rate and extent of cell expansion during diffuse, irreversible growth (Cosgrove, 2016; Cosgrove, 2018). One hypothesis to explain the observed defects in the rates and ranges of stomatal opening and closure in *PLL12* mutant plants is that in Col plants, *PLL12* cleaves HG in guard cell walls to prevent extensive pectin crosslinking, reducing wall modulus to facilitate stomatal opening and closure. Alternatively, *PLL12* might influence guard cell pressurization without changing wall modulus, or it might influence both properties. To resolve these hypotheses, real-time, simultaneous measurements of wall modulus and turgor pressure in guard cells during responses to physiological stimuli are necessary. However, such measurements have not yet been achieved in guard cells, which are small and undergo large changes in turgor pressure (Franks et al., 1998).

Advances in nanoindentation combined with finite element modeling (FEM), which have been employed to investigate the mechanics of epidermal cells of Arabidopsis and other systems (Bidhendi and Geitmann, 2019; Forouzesh et al., 2013; Li et al., 2021), now enable us to probe the mechanics of functioning guard cells. Nanoindentation directly and rapidly measures the force exerted between a probe tip and a cell indented sequentially at precise depths. With these data, local stiffness (force/length) can be quantified at specific depths. The local stiffness is governed by a combination of cell morphology, wall modulus, and turgor pressure. Thus, both wall modulus and turgor pressure can be estimated using a computational model (FEM) of the measurements. This model includes the measured shape of a given guard cell, with the model being used to characterize the relationship between the local stiffness and the probe indentation depth, wall modulus, and turgor pressure. This approach is effective because the local stiffness is depth dependent, with shallow indentations (less than the thickness of the wall) influenced more by wall modulus and deeper indentations influenced more by turgor pressure. By measuring stiffness values at different depths in the same location and using FEM, the wall modulus and turgor pressure at a given time

point can be estimated, and these measurements can be made repeatedly over the course of a physiological response experiment without killing the cell.

In our experiments, plants that had been kept in the dark overnight to induce stomatal closure were placed in a nanoindenter, and their stomata were induced to open and then to close by turning a light on and then off (Figure 2). Individual guard cells from attached leaves were indented every ten minutes or less (Figure 2A-B), and apparent stiffness at each specific depth was quantified from the unloading curve (Figure 2B). It should be noted that apparent stiffness increased soon after the light was turned on and dropped after the light was turned off for all the genotypes (Supplemental Figure 4).

To disentangle the contributions of wall modulus and turgor pressure to changes in apparent stiffness (Figure 2B) and stomatal aperture, each measurement for every cell was modeled using FEM. The model was constructed using measured cell size for each indented cell and wall thickness for each genotype (Supplemental Figure 5B-C). The cell wall was modeled as an anisotropic elastic material with circumferential (E2), longitudinal (E1), and radial (E3) moduli (Figure 2D). The E2 direction is aligned with the orientation of cellulose microfibrils (CMs) and was assumed to remain constant during the light on/off stages because guard cells undergo much less circumferential deformation than elongation during stomatal opening (Meckel et al., 2007). E1 and E3 moduli, which represent potential mechanical contributions from cellulose and wall matrix polymers, were assumed to be equal, were defined to be four times lower than E2 for the initial dark condition (see Methods; Marom et al., 2017; Yi et al., 2018), and were allowed to change during stomatal opening/closing. Simulations of nanoindentation measurements (Figure 2C) were performed iteratively (Figure 2E) to match each measured apparent stiffness as a function of indentation depth in order to estimate the E1 and E3 moduli, turgor pressure, and the geometrical deformation (Supplemental Figure 6A).

This analysis revealed that in Col guard cells, wall modulus increased significantly within five minutes after light stimulation, then diminished slowly during the light-on

phase; after light-off, the wall modulus in Col guard cells dropped suddenly then slowly recovered (Figure 2F and Supplemental Figure 6C). Turgor pressure in Col guard cells also increased rapidly when the light was turned on and continued to increase more slowly over the course of light stimulation; when the light was turned off, turgor pressure dropped promptly within the first five minutes and then continued to decrease (Figure 2G and Supplemental Figure 6E).

In *pll12-1* guard cells, wall modulus also rose immediately, then gradually increased upon light stimulation, with a sudden drop and gradual recovery after the light was turned off. However, E1 and E2 moduli in *pll12-1* guard cells were higher than in Col cells, both when stomata were closed in the first 20 min of the experiment, and after the light was turned on (Figure 2F and Supplemental Figure 6B). Conversely, turgor pressure in *pll12-1* guard cells was lower in the initial closed state, failed to increase as much within the first 5 minutes after light stimulation, and remained lower throughout the experiment than in Col cells (Figure 2G and Supplemental Figure 6F). In *PLL12OE* guard cells, no significant difference in wall modulus was detected in comparison to Col cells. However, turgor pressure initially dropped, then plateaued in *PLL12OE* guard cells after the light was turned off, a pattern that differed slightly from that in Col cells (Figure 2G). These abnormalities in wall modulus and turgor pressure dynamics in both genotypes were consistent with the results of the stomatal function assays, where *pll12-1* stomata opened less and slower than Col stomata in response to light (Supplemental Figure 3D, 3F) or FC (Figure 1C), and *PLL12OE* stomata opened normally but closed less than Col stomata in response to dark (Supplemental Figure 3C, 3E) or ABA (Figure 1A).

For comparison, we also measured turgor pressure in guard cells using incipient plasmolysis (Weber et al., 2015). Turgor pressure in guard cells was estimated in leaves exposed to light with fully open stomata and in leaves treated with ABA and darkness for 2.5 h to induce stomatal closure. Using incipient plasmolysis, turgor pressure values in guard cells of open and closed stomata were estimated to be 1.67 +/- 0.46 MPa and 0.65 +/- 0.02 MPa, respectively, in Col leaves; 4.58 +/- 1.13 and 3.30

+/- 0.81 MPa in *pll12-1* leaves; and 1.48 +/- 0.02 MPa and 0.90 +/- 0.08 MPa in *PLL12OE* leaves. These values for Col and *PLL12OE* guard cells were comparable to the maximal and minimal turgor pressure values derived from nanoindentation-FEM analyses (Figure 2G). However, turgor pressure values estimated by incipient plasmolysis for *pll12-1* guard cells were around three times those from nanoindentation-FEM analyses. The majority of the incipient plasmolysis results were consistent with the nanoindentation-FEM results with the exception of *pll12-1*, where changes in wall structure might inhibit osmolyte diffusion and/or water transport, complicating the estimation of turgor pressure by incipient plasmolysis, which is known to be time- and condition-dependent (Willmer & Beattie, 1978).

The sensitivity of FEM models to different E1:E2 modulus ratios was tested for single Col and *pll12-1* guard cells (Supplemental Figure 6G). Changing the E1:E2 ratio from 1:4 to 1:2 led to 3% and 25% increases in estimated turgor pressure, whereas changing the ratio to 1:8 resulted in 18% and 12% decreases in estimated turgor pressure, respectively. These changes are much smaller than the ~2-fold difference in estimated turgor pressure between Col and *pll12-1* guard cells (Figure 2G). Examining E1 and E2 values, we observed increases in E1 of 18% and 27% upon changing the E1:E2 ratio from 1:4 to 1:2, and decreases in E1 of 20% and 16% upon changing the E1:E2 ratio from 1:4 to 1:8 in Col and *pll12-1* guard cells, respectively. In contrast, E2 decreased by 41% and 36% upon changing the E1:E2 ratio from 1:4 to 1:2; whereas E2 increased by 59% and 68% upon changing the E1:E2 ratio from 1:4 to 1:8 in Col and *pll12-1* guard cells, respectively. As for turgor pressure values, these changes are smaller than difference in estimated E1 modulus between Col and *pll12-1* guard cells (Figure 2F).

To further examine the guard cell-specific function of *PLL12* in stomatal dynamics, nanoindentation-FEM analysis was performed on *PLL12kd2* and *GFPkd2* plants that were grown in the dark overnight. Estimated turgor pressure in *PLL12kd2* guard cells was significantly lower than in *GFPkd2* guard cells (Supplemental Figure 6H), whereas estimated wall modulus in *PLL12kd2* guard cells was similar to that in *GFPkd2* guard

cells (Supplemental Figure 6H). Together, these data imply that *PLL12* is required to establish normal cell pressurization and wall mechanics in guard cells to facilitate dynamic stomatal responses, and that the former of these depends on the expression of *PLL12* specifically in guard cells.

Changes in *PLL12* Expression Alter HG Composition in Guard Cell Walls

The above data reveal a physical mechanism by which *PLL12* modulates guard cell mechanics. A next step was to determine whether the molecular status of the cell wall correlated with these physical and functional changes in *PLL12* mutants. To test the hypothesis that PLL12 cleaves HG in the guard cell wall to alter the status of the pectin network and influence wall mechanics, guard cells of wild type and mutant genotypes were labeled with dyes and antibodies that recognize different forms of HG (Figure 3). Chitosan oligosaccharide-Alexa 488 (COS^{488}) interacts with low methyl-esterified (low DM) homogalacturonan (Mravec et al., 2014), and propidium iodide (PI) binds to negatively charged uronic acids in homogalacturonan (Rounds et al., 2011) (Figure 3A). The antibody 2F4 interacts with calcium cross-linked HGs (Liners, 1989; Powell et al., 1982), and LM19 and LM20 recognize low and high DM HG, respectively (Verhertbruggen et al., 2009) (Figure 3A). We also measured total uronic acid content in leaves to estimate the abundance of HG.

In *pll12-1* guard cells, COS^{488} labeling intensity was lower and 2F4 and PI labeling intensity were slightly but statistically significantly higher than in Col controls, but LM19 and LM20 labeling intensity did not differ from Col controls (Figure 3A-K). Total uronic acid (UA) content was slightly but not statistically significantly lower in *pll12-1* rosettes than in Col (Figure 3L). These results suggest that the walls of *pll12-1* guard cells contain less de-methylesterified HG that is available for COS^{488} binding, but higher amounts of calcium cross-linked HG. In guard cell walls of *PLL12 OE* plants, PI staining intensity was higher than in Col controls (Figure 3D-E), but labeling intensity with other probes and uronic acid content in leaves did not differ from Col (Figure 3B-C and F-L), suggesting that HG in guard cell walls of *PLL12OE* plants might contain more de-

methylesterified uronic acids. Uronic acid content was also higher in *PLL12OE* leaves than in *pll12-1* leaves (Figure 3L).

Altered wall composition in *pll12-1* and *PLL12OE* guard cells supports the influence of *PLL12* on HG abundance and modification status. To probe pectin metabolism further, we measured total PL, PG and PME activities in protein extracts from rosettes. No significant differences in the activities of these enzymes were detected across genotypes (Figure 3L), although these assays with total protein from leaves might obscure more specific changes in pectin metabolism in guard cells in relation to altered *PLL12* expression. Overall, the data in Figure 1-3 indicate that excessive HG crosslinking might account for the higher wall modulus observed in *pll12-1* guard cells that accompanies their defective stomatal opening and closure. In *PLL12OE* guard cells, slower stomatal closure and opening are accompanied by more subtle changes in cell biomechanics and wall composition.

Normal PLL12 Expression in Guard Cells is Required for Cell Proliferation but not Cell Expansion in Growing Rosette Leaves

The physiological function of *PLL12* was investigated by examining the sizes of 21-day old plants of different genotypes. Average rosette area in *pll12-1* plants was about one fifth of that in Col plants*,* and complementation with *PLL12* fully rescued the *pll12-1* dwarf phenotype (Figure 4). *PLL12OE* plants also had smaller rosettes than Col (Figure 4B-C). *GFPkd1* control plants had smaller rosettes than Col, and both *PLL12kd2* and *3,* but not *PLL12kd1*, plants had smaller rosettes than Col and *GFPkd2* and *3*, in keeping with qPCR data, where *PLL12kd2* and *3* but not *PLL12kd1* plants had significantly reduced *PLL12* transcript levels in rosette leaves (Supplemental Figure 2F).

We next sought to determine how *PLL12* affects rosette growth at the cellular level. Compared to Col controls, *pll12-1* plants showed ~20% and ~50% reductions in guard cell and pavement cell area, respectively, with an approximately two fold increase in stomatal density (stomata/area, Figure 4D-F) but no change in stomatal index (stomata/(stomata + pavement cells)). This smaller cell size alone does not account for

415 the 80% reduction in rosette area in the *pll12-1* mutant (Figure 4A-B), suggesting that
416 both cell expansion and proliferation might be affected. Restoration of *PLL12* rescued
417 these phenotypes in *PLL12comp* plants (Figure 4C-G). Despite their reduced leaf size,
418 cell size and stomatal patterning were unaltered in *PLL12OE* plants (Figure 4C-G).
419 Likewise, *PLL12kd2* plants did not show changes in cell size or stomatal patterning
420 (Figure 4C, H-K), implying that reduced rosette area in these plants (Figure 4A-B) arises
421 mainly from reduced cell proliferation.
422
423 **Discussion**
424
425 Here we report that in addition to polygalacturonase and pectin methylesterase genes
426 (Amsbury et al., 2016; Huang et al., 2017; Rui et al., 2017), a previously
427 uncharacterized PL gene, *PLL12*, also influences stomatal function. Although both PL
428 and PG genes encode enzymes that degrade demethylated HGs in the cell wall, loss of
429 *PLL12* alters stomatal dynamics differently from the loss of a guard cell-expressed PG,
430 *PGX3* (Rui et al., 2017). Whereas *pll12-1* stomata open and close slower over a smaller
431 dynamic range than Col stomata, *pgx3-1* knockout stomata open normally but close
432 with a slightly smaller dynamic range and in a step-wise fashion, potentially reflecting
433 differences in substrate specificity between the PL and PG. The higher amount of
434 calcium cross-linked HG in *pll12-1* cell walls as detected by 2F4 immunolabeling is
435 consistent with the canonical function of PLs in degrading pectate. Similarly, *pgx3-1*
436 walls show increased 2F4 labeling, suggesting that calcium cross-linked HG might be a
437 common substrate for both PL and PG enzymes (Rui et al., 2017). However, the
438 findings that LM19 labeling of low-methylesterified HG is increased in *pgx3-1* guard
439 cells but similar to controls in *pll12-1* mutants suggests that PLL12 might target a type of
440 HG that is distinct from that targeted by PGX3.
441
442 *PME6* is also required for stomatal function (Amsbury et al., 2016). A common
443 phenotype of *pme6-1* and *pll12-1* guard cells is that stomata in both mutants open and
444 close within a smaller dynamic range, but whereas *pll12-1* stomata could reach to more
445 closed state than WT, *pme6-1* stomata could not close (Amsbury et al., 2016). In

addition to having different enzymatic effects on the cell wall, turgor pressure dynamics might be differentially altered in these mutants. Further empirical and modeling analyses of additional genetic and/or biochemical perturbations of guard cell walls will be required to better understand how different classes of pectin-modifying enzymes influence guard cell mechanics and function (Amsbury et al., 2016; Jones et al., 2003).

The nanoindentation-FEM approach described here is a new method for simultaneously tracking wall modulus and turgor pressure in living guard cells undergoing physiological responses. For Col guard cells, E1 and E3 modulus values in the dark were estimated to be around 20 MPa (Figure 2F), which is very close to previous AFM measurements of apparent modulus in plasmolyzed guard cells (Carter et al., 2017). Upon light stimulus, we observed an immediate initial increase in directional wall modulus that slowly diminished over the course of light stimulation (Figure 2F). A study in tobacco stomata combining the use of a pressure probe to inflate guard cells with calculations of volumetric elastic modulus found that the bulk modulus of guard cells increases as stomata open wider (Zhang et al., 2011), and a theoretical analysis of wall mechanics predicted an increase in E2 in the guard cell wall during stomatal opening that was proposed to arise from strain-stiffening (Wu and Sharpe, 1979). Therefore, we suspect that the rapid initial increase in modulus we observed (Figure 2F) might be caused by strain stiffening of the wall (Cosgrove, 1993; Kierzkowski et al., 2012), whereas the subsequent slow reduction in modulus might represent time-dependent wall relaxation accomplished by wall-loosening proteins such as expansins (Cosgrove, 2016; Zhang et al., 2011). Together, our findings along with previous studies support the existence of dynamic changes in directional wall modulus during guard cell deformation, opening new avenues for studying the interplay between wall mechanics and cell wall remodeling during stomatal dynamics.

In Col plants, our nanoindentation-FEM analysis revealed an initially sharp, then gradual increase in turgor pressure from ~0.5 MPa to ~1.3 MPa over 60 min of light exposure that accompanied an increase in stomatal pore width of ~0.8 μm, (Figure 2G and Supplemental Figure 6A). These dynamic changes in turgor pressure are potentially

driven by initial rapid ion flux into guard cells upon light-induced membrane depolarization and a corresponding drop in osmotic potential that causes water influx, both of which fluxes slow but do not cease as guard cells continue to respond to the light stimulus (Jezek and Blatt, 2017). Likely due to their small size, there have been no prior reports of turgor pressure measurements for *Arabidopsis* guard cells. However, for species where guard cells have been probed, turgor pressure increases by ~0.25-1 MPa along with each ~1 μm increase in stomatal pore width (Franks et al., 1998), which is within the same order of magnitude as the turgor pressure-pore width correlation we report here.

The ability to capture dynamic changes in turgor pressure during stomatal opening and closure, especially the previously unreported rapid increase and decrease in turgor pressure we observed upon switching the light stimulus on or off, paves the way for investigation of the functional connections between rapid signaling events and turgor pressure in guard cells. The asymmetry we observed in both wall modulus and turgor pressure changes is further evidence for the cryptic hysteresis that is hypothesized to be a feature of guard cell biomechanics, in which biophysical hysteresis underlies the apparently symmetrical opening and closure behaviors of guard cells (Rui et al., 2017).

In *pll12-1* knockout plants, we found that although wall modulus and turgor pressure values in guard cells derived from nanoindentation-FEM analyses showed similar dynamic trends as in Col plants, wall moduli remained consistently higher, whereas turgor pressures were consistently lower than in Col guard cells. The nanoindentation-FEM results for *PLL12OE* plants were more complex, with wall modulus values lying in between values for Col and *pll12-1* but not differing significantly from either genotype at most timepoints, whereas turgor pressure in *PLL12OE* stomata was estimated to be nearly indistinguishable from Col, except for showing a slower reduction after lights off. We conclude that the observed dysfunctional stomatal dynamics in *pll12-1* plants (Figure 1) arise from the combined effects of stiffer cell walls and a smaller initial jump and slower increase in turgor pressure (Figure 2), while the observed slower stomatal closure in *PLL12OE* plants (Figure 1) arise from the slower decrease of turgor pressure

(Figure 2). The more closed stomata in *PLL12kd* lines than *GFPkd* lines after 2.5h ABA treatment or before FC treatment (Figure 1G and Supplemental Figure 3I-L) are attributable to a significant lower turgor pressure, but not wall modulus in *PLL12kd* lines (Supplemental Figure S6H).

Application of exogenous PG to guard cells reduces their apparent elastic modulus as measured by AFM (Carter et al., 2017), underscoring the importance of pectin modification in determining wall mechanics in guard cells. A higher proportion of cross-linkable HG in *pll12-1* (Figure 3) likely accounts for the observed increase in wall stiffness, as previous findings demonstrate that a higher proportion of calcium crosslinked pectins in pectin gels increases their elastic modulus *in vitro* (Ström et al., 2007). An AFM study of *Arabidopsis* hypocotyl cells also revealed a correlation between more abundant calcium-crosslinking pectin and higher wall modulus (Daher et al., 2018). The finding that wall modulus in guard cells is significantly increased in *pll12-1* plants but not in *PLL12kd2* plants might be attributable to remaining PLL12 activity in *PLL12kd* plants.

Our study showed that knocking out *PLL12* inhibits guard cell pressurization after light stimulus, whereas overexpressing *PLL12* prevents continued guard cell depressurization upon light removal (Figure 2G). Knocking down *PLL12* specifically in guard cells also reduces turgor pressure in guard cells (Supplemental Figure S6H), suggesting that maintaining stomatal pore aperture, which depends on guard cell pressurization, requires *PLL12* expression specifically in guard cells. These findings were unexpected and highlight a potential connection between HG degradation by PLs and signaling networks, such as cell wall integrity (CWI) sensing (Bai et al., 2009; Ma et al., 2019; Ringli, 2010), that include stomatal responses to pectin oligosaccharides (Lee et al., 1999). These results suggest that wall-modifying enzymes might affect cell mechanics and dynamic behaviors through a signaling-mediated influence on turgor pressure in addition to their direct effects on wall modulus, and demonstrate the need to measure both turgor pressure and wall modulus simultaneously in studies of stomatal

responses and to apply genetic and molecular tools to investigate how feedback from wall integrity signaling might influence wall mechanics.

Because pectins are thought to exist in complex three-dimensional networks whereas cellulose orientation is constrained within the plane of the cell wall, it is possible that altering *PLL12* expression changes directional wall moduli differently, a subject for further refinement and testing of the nanoindentation-FEM approach described here. In our FEM analysis, the ratio of E1:E2 wall modulus was assumed to be 1:4 for the closed state given the estimated proportions, physical properties, and orientations of cellulose and matrix polysaccharides in the guard cell wall (Marom et al., 2017; Yi et al., 2018). However, if pectin is the only polysaccharide affected in *pll12-1* plants, and more extensive pectin crosslinking in the guard cell wall gives rise to higher moduli in all dimensions, E1 would be expected to increase relative to E2, moving the E1:E2 ratio closer to or past 1:2. If the ratio were 1:2, turgor pressure in *pll12-1* guard cells would be 25% higher than our current estimation (Supplemental Figure S6G) but would still be lower than in Col guard cells (Figure 2G).

We also employed incipient plasmolysis for comparison with our nanoindentation-FEM analyses. Turgor pressure estimates obtained for Col and *PLL12OE* were similar between the two methods. Additionally, the difference in turgor pressure between open and closed stomata, as estimated by incipient plasmolysis, was smaller in *PLL12OE* guard cells (0.58 MPa) than in Col guard cells (1.02 MPa). This result is consistent with the slower decrease in turgor pressure in PLL12OE guard cells than Col after light was turned off, as suggested in nanoindentation-FEM analysis, although that difference was not statistically significant (Figure 2G). However, the turgor pressure values estimated in guard cells of *pll12-1* knockout plants with open and closed stomata were about three times the values obtained by the nanoindentation-FEM analysis. This discrepancy raises the possibility that the nanoindentation-FEM approach does not accurately derive turgor pressure in the *pll12-1* mutant in contrast to the highly-correlated results for other genotypes as well as pavement cells (Li et al., 2021). Instead, we think it is more likely that turgor pressure in the *pll12-1* mutant is less able to be accurately measured by

incipient plasmolysis, because that method depends on factors such as plasmolysis time, solute identity, and diffusion rates of water and solutes (Willmer & Beattie, 1978). The altered stomatal behavior and wall composition observed in *pll12-1* further complicate interpretations of incipient plasmolysis data. In contrast, nanoindentation is rapid and FEM takes into account differences in cell geometry between genotypes, highlighting its utility for estimating turgor pressure in guard cells.

We found that *PLL12* affects rosette size by affecting both cell expansion and proliferation (Figure 4), which is consistent with the function of a rice PLL gene, *DEL1*, in cell cycle progression and leaf growth (Leng et al., 2017). However, another Arabidopsis PL gene, *PMR6*, affects cell expansion but not proliferation (Vogel, 2002). PL genes might potentiate cell expansion by loosening the pectin network in the wall in a mechanism comparable to that of PGs (Rui et al., 2017; Xiao et al., 2014). Alternatively, *PLL12* might function in cell expansion by helping to establish the molecular architecture required to maintain proper wall integrity (Anderson, 2016; Leng et al., 2017). Defects of the *PLL12kd* line in cell proliferation but not expansion suggest that *PLL12* influences cell proliferation in a guard cell-specific manner to influence rosette growth, potentially by simply enabling sufficient CO_2 capture through stomata to drive photosynthesis and provide energy for leaf cell proliferation. Our findings suggest a dual role for PLL12 in rosette leaf growth, in that it might facilitate guard and pavement cell expansion by degrading pectin and enable cell proliferation by potentiating stomatal dynamics.

In summary, we found that the putative pectate lyase, PLL12, reduces levels of cross-linkable HG in the guard cell wall and is required for the ability of guard cells to maintain sufficient turgor pressure for driving guard cell expansion in response to light. By enabling normal stomatal function, guard cell-expressed *PLL12* influences cell proliferation and leaf growth. The ability to measure stomatal biomechanics in real time and combine realistic models of guard cells with sophisticated material simulations has allowed us to shed light on the unexpected biophysical mechanisms by which stomatal guard cells respond to external stimuli, and have revealed how a cell wall-modifying

gene influences guard cell biomechanics and stomatal dynamics. Further dissection of these mechanisms will enable plant improvement for the development of resilient and sustainable crops that will benefit human societies.

Methods

Generation of transgenic plants

Seeds of wild-type Arabidopsis Col-0 and T-DNA insertion mutant *pll12-1* (CS878465) were obtained from ABRC. To constitutively overexpress *PLL12*, *PLL12* coding sequence (PCR by primer *PLL12*F and primer *PLL12*R) was cloned into entry vector pCR8/GW/TOPO using a TA Cloning Kit; then the coding sequence was inserted into destination vector pEarleyGate 101 using Gateway LR Clonase II (Invitrogen); the overexpression construct was then transformed into the Col-0 background and homozygous plants were selected using 5 μM methionine sulfoximine. For *PLL12* expression pattern analysis, a 2 kb fragment upstream of the *PLL12* start codon (PCR by primer p*PLL12* F and primer p*PLL12* R) was TA cloned into the pCR8/GW/TOPO entry vector and then LR cloned into pMDC162 which contains a GUS coding sequence; the plasmid was then transformed into Col-0, and transgenic plants were selected on 25 μg/mL hygromycin to obtain homozygous lines. To generate the *PLL12* complementation line, the 2 kb *PLL12* native promoter and *PLL12* coding sequence described above were ligated (primer *PLL12* p/CDS overlap) and cloned into the pCR8/GW/TOPO entry vector, then LR cloned into vector pMDC110 (Curtis and Grossniklaus, 2003); the plasmid was transformed into *pll12-1* heterozygous plants then selected by using 5 μM methionine sulfoximine and 25 μg/mL hygromycin to obtain homozygous lines for both alleles. To obtain guard cell-specific knockdown lines and technical controls, amiRNAs targeting three different sites of *PLL12* and *GFP* were designed (see key resource table) and inserted into vector pMDC32B-AtMIR390a-B/c separately (Carbonell et al., 2014), the 35S promoter on the vector was replaced by the guard cell specific promoter *pGC1* (PCR using primers pGC1 D1 F and pGC1 D1 R and restriction enzymes PstI and KpnI, T4 DNA ligase (NEB)) (Yang et al., 2008) to achieve cell-specific expression of amiRNAs. Plant transformation was performed using an agrobacterium (*GV3101*)-based floral dip method.

631

632 Plant growth conditions

633 Surface sterilized (20 min in 30% bleach + 0.1% SDS) *Arabidopsis thaliana* seeds were
634 stratified at 4 deg C for 3-10 days before being plated on Murashige and Skoog (MS)
635 plates containing 2.2 g/L Murashige and Skoog salts (Caisson Laboratories), 0.6 g/L
636 MES, 1% (w/v) Suc, and 0.8% (w/v) agar (Sigma), pH 5.6. Seedlings were grown at
637 22°C under 24 h of illumination for 10 days before being transferred to soil
638 supplemented with Miracle-Gro (The Scotts Company). Plants were grown in a chamber
639 under 16-h-light/8-h-dark light conditions at 22°C.

640

641 Gene expression analysis

642 For GUS staining, 6-day-old seedlings, epidermal peels or rosettes of 3-4-week-old
643 *PLL12* pro::GUS lines were soaked in GUS staining solution (50 mM sodium phosphate,
644 pH 7.2, 0.2% (v/v) Triton X-100, and 2 mM X-Gluc) in the dark for 3-16 h before de-
645 staining with 70% ethanol. A Zeiss Discovery V12 fluorescence dissecting microscope
646 was used to collect images of seedlings; a Zeiss Axio Observer microscope attached to
647 a Nikon D5100 DSLR camera was used for the epidermis, and a Scanjet 8300 scanner
648 (HP) at 600 dpi was used for rosette imaging.

649 For qPCR, total RNA was extracted from 21-day-old rosette leaves 5-8 using a
650 NucleoSpin RNA Plant kit (Machery-Nagel) and cDNA was synthesized using Quanta
651 qScript cDNA Supermix (Quantabio). The cDNA and PLL12 qPCR primers (*PLL12*qF
652 and *PLL12*qR) were mixed with Quanta PerfeCTa SYBR Green Fastmix ROX
653 (Quantabio; catalog no. 95073-250). Reactions and quantification were performed on a
654 StepOne Plus Real-Time PCR machine (Applied Biosystems). To calculated the relative
655 expression of *PLL12* across different transgenic plants, *ACTIN2* (*ACT2*) (ACT2-qF and
656 ACT2-qR) and Col-0 were used as controls.

657

658 Plant growth analysis

659 Twenty-one-day-old plants were imaged with a Nikon D5100 DSLR camera. Images
660 were segmented based on color threshold: images were opened in ImageJ and based
661 on the HSV (Hue, Saturation, and value) color space, green regions were selected to

separate rosettes from the background. Afterward, the background was removed and the wand tool was used to select each rosette to measure its area. For the epidermal cell dimension and patterning study, leaves 5-8 from 21-day-old plants are excised and imaged. To measure guard cell size, the epidermis of a leaf was peeled and soaked in 100 μg/mL Propidium Iodide (PI) for 5 min. For pavement cell size and stomatal density and index, intact leaves were used. Images were collected on a Zeiss Axio Observer microscope with a Yokogawa CSU-X1 spinning disk head using a 63X 1.4 NA oil immersion objective for guard cell size and a 20X 0.5 NA air objective for other measurements. A 561 nm excitation laser and a 617/73 nm emission filter were used to image PI. Five fields of three plants per genotype were imaged and quantified using ImageJ.

Stomatal function assays

Fully expanded mature leaves (leaves 5-8 from 3-4-week-old plants) were excised and used for stomatal function assays (Rui and Anderson, 2016). To record stomatal opening responses to FC, excised leaves were acclimated in dark solution (20 mM KCl, 1 mM $CaCl_2$, and 5 mM MES-KOH, pH 6.15) for 2.5 h, then leaves were incubated in 1 mM FC in dark solution in the dark for another 2.5 h. To record stomatal closure responses to ABA, excised leaves were acclimated in light solution (containing 50 mM KCl, 0.1 mM $CaCl_2$, and 10 mM MES-KOH, pH 6.15) for 2.5 h, then leaves were incubated in 50 mM ABA contained light solution in light condition for another 2.5 h. To track stomatal opening response to light, excised leaves were acclimated in light solution (containing 50 mM KCl, 0.1 mM $CaCl_2$, and 10mM MES-KOH, pH 6.15) for 2.5 h in the dark, then transferred to the light for another 2.5 h. To record stomatal closure responses to dark, excised leaves were acclimated in dark solution (20 mM KCl, 1 mM $CaCl_2$, and 5 mM MES-KOH, pH 6.15) for 2.5 h in the light, then transferred to the dark for another 2.5 h. For Col, *pll12-1, PLL12OE, GFPkd2,* and *PLL12kd2,* epidermises from two leaves of each genotype were peeled every 30 min and imaged; for pore width comparison in *GFPkd1-3* and *PLL12kd1-3*, epidermises were peeled and collected 0 min and 150 min after ABA or FC incubation. Samples were imaged on a Zeiss Axio Observer microscope; ten fields per epidermis were imaged. Each assay was repeated

693 at least three times and in each experiment, epidermises were peel from two leaves
694 from two individual plants. Stomatal pore area, complex area, and pore width were
695 measured using ImageJ. To account for different guard cell sizes, especially in *pll12-1*,
696 area ratio (pore area / complex area) was calculated and displayed to reflect the degree
697 of stomata opening.
698
699 HG labeling of intact guard cells
700 Fully expanded mature leaves (leaves 5-8 from 3-4-week-old plants) were used for both
701 COS488 and PI labeling.
702 For COS488 staining (Mravec et al., 2014), epidermises were peeled and stained in a
703 1:1000 diluted solution for 20 min, and after rinsing, z-stack images (0.5 μm z distance)
704 were taken using a 488-nm excitation laser and a 525/50-nm emission filter. For PI
705 staining, epidermises were peeled and stained in 100 μg/ml PI for 5 min, and after
706 rinsing away excess dye, z-stack images (0.5 μm z distance) were taken using a 561-
707 nm excitation laser, and a 617/73-nm emission filter. Images were collected with a Zeiss
708 Axio Observer microscope with a 63X 1.4 NA oil immersion objective. To quantify
709 fluorescence intensity, z-stack images were projected using the SUM algorithm in
710 ImageJ, then areas and raw integrated density of entire guard cell regions for COS488
711 labeling and guard cell regions without phenolic rings for PI staining were measured.
712 Relative fluorescence intensity was calculated by dividing raw integrated density by
713 traced area.
714
715 Immunolabeling and dye staining of guard cell cross-sections
716 For section preparation, square 3 mm leaf patches cut from leaves were soaked in 4%
717 (w/v) formaldehyde in PEM buffer (0.1 M PIPES, 2 mM EGTA, 1 mM $MgSO_4$, pH 7) by
718 vacuum infiltration then incubated for 1 h (Rui et al., 2017). The leaf patches were then
719 dehydrated in an ethanol series (30 min each in 30%, 50%, 70%, 100% ethanol) and
720 infiltrated with LR White Resin (Electron Microscopy Science) diluted in ethanol (30 min
721 each in 10%, 20%, 30%, 50%, 70%, 90%, and 100%); 100% LR White Resin was
722 replaced two more times with at least 8 h incubations. Samples were placed vertically in
723 gelatin capsules (Ted Pella) filled with resin for 7 days at 37°C. Sections of 2 μm

724 thickness were cut using a Leica UC6 ultramicrotome with a glass knife and collected
725 on positively charged glass slides. For immunolabeling, sections were blocked in 3%
726 (w/v) BSA in KPBS (0.01 M K_3PO_4 and 0.5 M NaCl, pH 7.1) for LM19 and LM20 labeling,
727 or in TCaS buffer (20 mM Tris-HCl, 0.5 mM $CaCl_2$, and 150 mM NaCl, pH 8.2) for 2F4
728 labeling, for 4 h. Sections were then incubated with a ten-fold dilution of primary
729 antibodies in 3% (w/v) BSA in KPBS or TCaS for 24 h at room temperature. After rinsing
730 three times with KPBS or TCaS solution, sections were incubated in secondary antibody
731 (100-fold dilution in in 3% (w/v) BSA in KPBS or TCaS) for 16 h. For LM19 and LM20,
732 the secondary antibody Alexa Fluor 488-conjugated goat anti-rat IgG (H+L), was used;
733 for 2F4, Alexa Fluor 488-conjugated goat anti-mouse IgG (H+L) was used. Samples
734 were rinsed three times again before being counterstained with 0.1% (w/v) S4B in
735 (KPBS or TCaS) for 30 min. After rinsing with KPBS or TCaS, samples were imaged
736 under Zeiss Axio Observer microscope with a 100X 1.4 NA oil objective. A 488-nm
737 excitation laser and a 525/50-nm emission filter were used for Alexa Fluor 488 signals,
738 and a 561-nm excitation laser and a 617/73-nm emission filter were used for S4B signal.
739 To quantify the arbitrary fluorescence units (AFU), the area of the guard cell wall was
740 traced using the S4B staining image, and raw integrated density from the same region
741 was measured. To account for background noise, AFU of samples that were stained
742 with only secondary antibody was also calculated and subtracted from the AFU of
743 samples with both primary and secondary antibody.
744 Measuring cell wall thickness was performed by staining sections prepared as for
745 immunolabeling with 0.05% (w/v) toluidine blue for 10–30 s and rinsing with water.
746 Samples were imaged using a Zeiss Axio Observer microscope with a 100X 1.4 NA oil
747 objective and a Nikon D5100 DSLR camera. Thicknesses of guard cell walls at different
748 positions were measured using ImageJ. Sections were prepared from three leaves from
749 three individual plants.
750
751 Enzymatic assays
752 Total protein extraction for PL activity assays was adapted from (Silva-Sanzana et al.,
753 2019). Rosettes of 4-5-week-old plants were ground in extraction buffer (1 M NaCl, 0.2
754 M Na_2HPO_4, 0.1 M citric acid, pH 6.5) then incubated at 4°C for 1.5 h. The homogenate

was then centrifuged at 15000 g for 10 min at 4°C, and the supernatant was then transferred to a new tube and centrifuged again, and the supernatant was used for the PL activity assay. A Bradford assay was used to measure protein concentration. Total protein was incubated with 0.12% (w/v) polygalacturonic acid (Sigma) in a solution containing 30 mM Tris-HCl pH 8.5 and 0.15 mM $CaCl_2$ at room temperature, and absorbance at 237 nm was measured every minute for 10 min. PL activity was defined as the increase in 237 nm absorbance per min per amount of total protein.

Total protein extraction for PG activity assays was performed as in (Xiao et al., 2014). Rosettes of four-to-five-week-old plants were ground in liquid N_2, and the powder was incubated in protein extraction buffer (50 mM Tris-HCl, 1 M NaCl, 3 mM EDTA, 2.5 mM 1,4-dithiothreitol (Sigma-Aldrich), 2 mM phenylmethylsulfonyl fluoride (Sigma-Aldrich), and 10% (v/v) glycerol, pH 7.5) for 1 h. The mixture was dialyzed in 50 mM sodium acetate buffer (pH 5.0) at 4°C for 16 h. Protein concentration was measured using a Bradford assay. PG activity was quantified by measuring the release of reducing ends. The dialyzed total protein was incubated with 0.5 % (w/v) polygalacturonic acid in 37.5 mM NaOAc (pH 4.4) at 30°C for 3 h, then 100 mM sodium tetraborate buffer (pH 9.0) and 200 µl 1% (w/v) 2-cyanoacetamide were added to label reducing ends. D-galacturonic acid (Sigma) was used as a standard. PG activity was defined as the amount of reducing ends produced per minute per amount of total protein.

A PECTOPLATE assay was used to measure PME activity (Lionetti, 2015). Total protein was extracted as for the PG activity assay. PECTOPLATEs contained 0.1% (w/v) apple pectin (Sigma), 1% (w/v) SeaKem LE Agarose, 12.5 mM citric acid, 50 mM Na_2HPO_4 at pH 6.5. Twenty microliters of 25 µg/mL protein samples were loaded in wells made by punching the PECTOPLATE with a cork borer with a 5 mm diameter. After incubation at 30°C for 16 h, plates were stained with 0.05% (w/v) Ruthenium Red (Sigma) for 30 min, then rinsed with water at least three times until halos were clear for imaging. Photos were taken using a Scanjet 8300 scanner (HP) and halo area was measured using Image J. A standard curve of PME activity and halo area was made using commercial PME (Prozomix PO).

Nanoindentation

A Hysitron Triboscan (Ti950, USA) was used to conduct nanoindentation experiments. The machine was equipped with a 50X objective so that guard cells could be easily identified. The diameter of the conical type tip of the probe is 2~3 μm. The tip was scanned using a confocal microscope and its geometry rendered for the computational model. A set force of 2-5 μN was used to engage each targeted cell. Displacement control was set for the input load function (Forouzesh et al., 2013), and the loading rate was 100 nm/s. As the indentation depth increased from 150 nm to 1250 nm, the contact area was estimated to increase from ~1.77 μm^2 (with a diameter of ~1.5 μm) to ~11.34 μm^2 (with a diameter of ~3.8 μm). The corresponding change to the internal cell volume caused by the indentations increased from ~1% to ~6.5% of the total cell volume. For the maximum indentation depth of 1250 nm, the effect of the neighboring cells in the local cell wall mechanical response was not substantial (Mosca et al., 2017; Li et al., 2021). Two blue bulbs (40 W each) were positioned in front of the probe at a distance of 14-15 inches to provide 200-250 $\mu mol/m^2 \cdot s$ light intensity. The door of the instrument was covered with foil to ensure dark conditions. To provide the blue light needed to activate guard cells, the front door of the machine was opened. Before testing, the leaf was mounted on a support using epoxy, then was put in a dark growth chamber for more than 12 hours. Then the sample was settled for 1-2 hours on the stage of the nanoindenter before testing. The lighting illumination of the microscope was set to a minimum level to reduce its effect on the guard cells. The middle of each guard cell from the top view was set as the indentation position. Indentation was performed every 5-10 min. For each genotype, experiments were performed using nine guard cells from five plants.

Finite element modeling (FEM)

Mechanical analysis of nanoindentation experiments was conducted using commercial finite element software (Abaqus, 2019) to estimate the wall modulus and turgor pressure of the cell. A structural model of each guard cell was constructed with the LOFT method in Abaqus using the polar length, complex width and guard cell width

817 evaluated from the optical image of the nanoindenter microscope. The thickness
818 distribution of the cross-section of the cell was set based on previous measurements
819 (Supplemental Figure 5-B). Similar to previous studies (Marom et al., 2017; Yi et al.,
820 2018), a linear anisotropic elastic model (transverse isotropy) was assigned uniformly
821 across the whole cell, and based on the estimated proportions, physical properties, and
822 orientations of cellulose and matrix polysaccharides in the guard cell wall, the
823 anisotropic modulus was assumed to have a relation E1:E2:E3=1:4:1 for the closed
824 state. E2 defined the wall modulus along the circumferential direction of the cell.
825 Poisson's ratios were set to $v_{12}=v_{23}=0.3$, and $v_{13}=0.47$. Shear modulus was assumed to
826 have a relation G12=G23=E1, and G13 can be determined by $G13=E1/(0.5+ v_{13})$. As a
827 result, only two unknowns, turgor pressure and modulus E2, need to be determined. For
828 boundary conditions, the materials at the polar positions were confined, ventral edges
829 were free of constraint, and dorsal edges were constrained in the vertical direction to
830 represent constraints from adjacent pavement cells. The analysis was conducted in two
831 steps: cell pressurization and nanoindentation. The pore width at the end of the
832 pressurization and the stiffness at shallow and deep indentation depths were used to
833 compare with experimental measurements iteratively. Once the optical and mechanical
834 measurements were matched, the turgor pressure and the cell wall modulus were
835 estimated.
836
837 For measurements of pore width (Supplemental Figure 5C) used in the FE analyses,
838 pore width in the first dark phase was obtained by subtracting the pore width of stomata
839 that were plasmolyzed by incubation in 1-3 M sorbitol for 1 h (turgor pressure is about 0
840 MPa) (see source data) from the stomata that were left under dark overnight (dark
841 phase). Pore width in the light phase and the second dark phase were estimated using
842 the stomatal opening and closure rate as determined using the stomatal function assay
843 results for light and dark treatments (Supplemental Figure 5C).
844
845 Incipient plasmolysis
846 Leaves were excised directly from 3-4-week-old plants that were growing under light to
847 constitute an open stomata group. To induce stomatal closure, excised leaves were

848 treated with 50 mM ABA in the dark for 2.5 h. Leaves with open or closed stomata were
849 soaked in 0.1 mM FM1-43 in sorbitol solutions of differing concentrations (0 M, 0.2 M,
850 0.4 M, 0.6 M, 0.8 M, 1 M for Col and *PLL12OE*, 0 M, 1 M, 2 M, 2.5 M, 3 M, 4 M for *pll12-*
851 *1*) for 40 min before imaging under a Zeiss Axio Observer microscope with a 63X 1.4
852 NA oil immersion objective. Z-stack images (0.5 μm z interval) were collected using a
853 488 nm excitation laser and a 525/50 nm emission filter. ImageJ was used to quantify
854 and calculate the ratio of plasmolyzed:total guard cells. A function of the ratio to sorbitol
855 concentration was plotted using DESMOS and fitted to an S curve, and the
856 concentration of sorbitol at the point where 50% of guard cells are plasmolyzed was
857 estimated and used to calculate turgor pressure as the osmotic potential at incipient
858 plasmolysis according to the equation $\Psi = c \cdot R \cdot T$, where c is the concentration of
859 sorbitol, R is the ideal gas constant (8.314 kPa·L/mol·K), and T is the temperature in
860 Kelvin (298 K). For both open stomata and closed stomata groups, nine leaves were
861 imaged and quantified for each sorbitol concentration.
862
863 Quantification and statistical analysis
864 Statistical analysis in this study was conducted with Graphpad. Protein alignment was
865 performed using the MAFFT plugin implemented in Geneious. DESMOS was used to
866 derive the sorbitol concentration at which guard cells are incipiently plasmolyzed.
867
868 **Data and code availability**
869 Further information and requests for vectors, transgenic plants constructed in the study
870 will be fulfilled by the corresponding author. Modeling and analysis code will be provided
871 upon request.
872
873 **Acknowledgments**
874 Thanks to Silu Shen, Rayna Marshall and Katya Iatsenko for help with data analysis, Dr.
875 Jozef Mravec for the gift of COS^{488}, Missy Hazen and Gang Ning in the Huck
876 Microscopy Core Facility at Penn State for technical support, and Dr. Yue Rui, Dr.
877 Daniel Cosgrove, Dr. Hojae Yi, and members of the Anderson lab for helpful
878 discussions. This work was supported by the National Science Foundation under Grant

MCB-1616316 awarded to C.T.A., James Z. Wang, and Virendra M. Puri. Nanoindentation measurements were performed at the UNL Nano-Engineering Research Core Facility (NERCF), which is partially funded by the Nebraska Research Initiative.

Author Contributions:

Y.C. and C.T.A. designed the project; Y.C. generated plant material and characterized plant growth, stomatal responses and cell wall modifications; W.L. and J.A.T. designed and developed the iterative experimental-computational method to analyze nanoindentation data; W.L. performed nanoindentation experiments and FE analysis; Y.C. and C.T.A. wrote the manuscript; Y.C., W.L., J.A.T. and C.T.A. edited the manuscript.

Figure Legends:

Figure 1. Expression of *PLL12* Affects Stomatal Function.

(A) Stomatal responses to 50 μM ABA in Col (black), *pll12-1 (magenta)* and *PLL12OE* (green) genotypes. Error bars indicate SEM; n ≥ 121 stomata per genotype per time point from three independent experiments. Different letters at each timepoint indicate P < 0.05 across genotypes for that timepoint, one-way ANOVA analysis and Tukey test (dashed gray box indicates statistical comparison group). (B) Representative images of stomata in Col*, pll12-1* and *PLL12OE* plants before and after 2.5 h ABA treatment. Stomatal complexes and pores are outlined by yellow dashed lines. Bar = 5 μm. (C-D) as in (A-B) but treated with 1 μM FC and n ≥ 122 stomata per genotype per timepoint. Bar = 5 μm. (E) Comparison of stomatal responses to 50 μM ABA between GFP kd-2 (black) and PLL12 kd-2 (blue) plants. Error bars indicate SEM; asterisks indicate significant difference between genotypes at each time point examined: **** P < 0.0001, Student's t-test; n ≥ 102 stomata per genotype per time point from three independent experiments and six biological replicates in total. (F) As in (B) but for GFP kd-2 and PLL12 kd-2. Images without outlines of PLL12 kd2 are also shown. Bar = 5 μm. (G-H) As in (E-F) but treated with 1 μM FC and n ≥ 112 stomata. Bar = 5 μm.

Figure 2. Altered *PLL12* Expression Affects Turgor Pressure More Than Wall Modulus in Guard Cells.

(A) Illustration of stiffness measurements by nanoindentation and experimental set up. Plants were kept in the dark overnight to ensure stomatal closure, and nanoindentation was performed at least every 10 min during the experiment. At 20 min after the first measurement (T0), light was turned on for 60 min to induce stomatal opening, then the light was turned off and measurements were collected for 30 min. The abaxial side of leaf seven was gently twisted to face upward, a target guard cell was located under the microscope, then the nanoindentation probe (tip radius = 2~3 μm) was moved to the same location. At each time point, stiffness in the same guard cell was measured at six different depths (B). (B) Diagram of indentation at different depths, representative force - depth curve for one guard cell, and definition of stiffness. Loading - unloading curves of all six different depths are shown by blue numbers. A zoomed in view of a loading (orange) and unloading (blue) curve at the fifth depth is shown in the blue box. Stiffness is defined as the slope of the unloading curve. (C) Simulation of calculated stiffness to six different depths. Blue dots represent the calculated stiffness from nanoindentation measurements; dashed line represents the results of the simulation. Bars = SD. (D) Representative FEM models. Upper and lower images represent modeled guard cell shapes before (dark) and after pressurization (light), respectively. Longitudinal modulus E1 was set to be the same as radial modulus E3, and both are four times smaller than circumferential modulus E2. (E) Illustration of iteration process to derive turgor pressure and wall modulus from nanoindentation simulation and FEM. (F-G) Wall modulus (F) and turgor pressure (G) derived for each genotype. n = 9 guard cells from at least five plants per genotype. Different letters at each timepoint indicate $P < 0.05$ across genotypes for that timepoint, two-way ANOVA analysis and Tukey test. Bars = SEM; ns = no significant difference.

Figure 3. *PLL12* Influences HG Labeling in Guard Cell Walls.

(A) Diagram showing different epitopes of HG that are recognized by the dyes and antibodies. Blue pentagon represents GalA, with or without red circle on Gal represents

941 methylated or unmethylated GalA. Yellow square represents PI molecule. (B)
942 Representative XY (upper panel) and XZ (lower panel) maximum projection images of
943 COS488 labeling. Images are displayed with a fire look-up table, XZ projections were
944 made from the midline in the Y direction. Bar = 5 µm. (C) Quantification of relative
945 intensity of COS488 labeling in guard cells from 3- to 4-week-old Col*, pll12-1* and *PLL12*
946 *OE* plants. Whiskers extend to min and max, box boundaries indicate first and third
947 quartiles of datasets, and horizontal lines inside boxes represent medians; n ≥ 153
948 guard cells per genotype from two independent experiments, six plants in total. Different
949 letters indicate $P < 0.05$, one-way ANOVA and Tukey test. (D-E) as in (B-C) but stained
950 with Propidium Iodide (PI) and n ≥ 131 guard cells per genotype. (F) Representative
951 images of cross sections of guard cells from Col*, pll12-1* and *PLL12 OE* plants,
952 immunolabeled with 2F4 (green) and counterstained with S4B (magenta). Bars = 5 µm.
953 (G) Quantification of 2F4 labeling intensity in cross-sections of guard cells from 3- to 4-
954 week-old Col*, pll12-1* and *PLL12 OE* plants. Error bars indicate SEM; n ≥ 112 guard
955 cells per genotype from at least two independent experiments, three different leaves.
956 Different letters indicate $P < 0.05$, or no significant differences across genotypes, one-
957 way ANOVA and Tukey test. (H-K) as in (F-G) but labeled with LM19 (H-I) or LM20 (J-
958 K). (L) Uronic acid content, and PL (pectate lyase), PG (polygalacturonase) and PME
959 (pectin methylesterase) enzymatic activity in Col, *pll12-1*, and *PLL12 OE* rosettes. For
960 uronic acid content, PG, and PME assays n = three independent experiments each with
961 five technical replicates per genotype. For the PL assay, n = three independent
962 experiments each with three technical replicates per genotype. Values are mean ± SD.
963 Different letters indicate $P < 0.05$, one-way ANOVA and Tukey test.
964
965 **Figure 4. *PLL12* Expression Affects Plant Growth, Epidermal Cell Expansion and**
966 **Proliferation.**
967 (A) Representative rosette images of 21-d-old Col, *pll12-1*, *PLL12* overexpression
968 (*PLL12 OE*), *PLL12* complementation (*PLL12 comp*) and guard cell-specific knockdown
969 pGC1::GFP kd-1 to -3 and pGC1::PLL12 kd-1 to -3 lines. Bar = 1 cm. (B) Rosette areas
970 of 21-d-old Col and *PLL12* transgenic plants; n≥35 plants per genotype from three
971 independent experiments. (C) Representative images of epidermal cells stained with

Propidium Iodide in 21-d-old *Col, pll12-1, PLL12 OE, PLL12 comp, GFP kd-2* and *PLL12 kd-2* plants. Enhance contrast was performed on the maximum projection of z-stack images. Bar = 100 µm. (D-G) Quantification of guard cell area (D), pavement cell size (E), stomatal density (F) and stomatal index (G) in 21-d-old Col*, pll12-1, PLL12 OE, PLL12 comp* plants. n ≥ 74 (D) and n ≥ 99 (H) guard cells from three individual plants per genotype. n ≥ 223 (E) and n ≥ 105 (I) pavement cells from at least three individual plants per genotype. n = three individual plants (F-G and J-K) with five fields of each were imaged and quantified for density and index analysis. Stomatal index = number of stomata (n_s) divided by the sum of stomata number and pavement cell number (n_p) per field ($n_s/(n_s+n_p)$). Different letters denote $P < 0.05$, one-way ANOVA and Tukey test. (F-I) as in (B-E) but for *GFP kd-2* and *PLL12 kd-2* plants. Dark gray dots or box represent Col, magenta for *pll12-1*, blue for *PLL12comp*, green for *PLL12OE*, light gray for *GFPkd*, and pink for *PLL12kd*. Error bars indicate SD. Whiskers extend to min and max, box boundaries indicate first and third quartiles of datasets, and horizontal lines inside boxes represent medians.

Supplemental Figures:

Supplemental Figure 1: *PLL12* encodes a putative pectate lyase in *Arabidopsis thaliana*.

(Supports Figure 1).

Supplemental Figure 2: *PLL12* is widely expressed in *Arabidopsis thaliana*.

(Supports Figure 1).

Supplemental Figure 3: PLL12 also functions in stomatal response to light conditions, and its function in stomatal response to ABA and FC is partially guard cell expression-dependent.

(Supports Figure 1).

Supplemental Figure 4: Apparent stiffnesses of Col, *pll12-1*, and *PLL12OE* guard cells at all depths.

(Supports Figure 2).

Supplemental Figure 5: Guard cell wall thickness used for FE analysis.

(Supports Figure 2).

Supplemental Figure 6: Additional FE analysis for guard cells in Col, *pll12-1* and *PLL12OE*.

(Supports Figure 2).

Supplemental Figure 7. Negative controls of immunolabeling in guard cell walls.

(Supports Figure 3).

REFERENCES

Amsbury, S., Hunt, L., Elhaddad, N., Baillie, A., Lundgren, M., Verhertbruggen, Y., Scheller, H.V., Knox, J.P., Fleming, A.J., and Gray, J.E. (2016). Stomatal Function Requires Pectin De-methyl-esterification of the Guard Cell Wall. Curr Biol *26*, 2899-2906.

Anderson, C.T. (2016). We be jammin': an update on pectin biosynthesis, trafficking and dynamics. J Exp Bot *67*, 495-502.

Aylor, D.E., Parlange, J.-Y., and Krikorian, A.D. (1973). STOMATAL MECHANICS. American Journal of Botany *60*, 163-171.

Babu, Y., and Bayer, M. (2014). Plant Polygalacturonases involved in cell elongation and separation—the same but different? Plants *3*, 613-623.

Bai, L., Zhang, G., Zhou, Y., Zhang, Z., Wang, W., Du, Y., Wu, Z., and Song, C.P. (2009). Plasma membrane-associated proline-rich extensin-like receptor kinase 4, a novel regulator of Ca2+ signalling, is required for abscisic acid responses in Arabidopsis thaliana. The Plant Journal *60*, 314-327.

Beauzamy, L., Derr, J., and Boudaoud, A. (2015). Quantifying hydrostatic pressure in plant cells by using indentation with an atomic force microscope. Biophysical journal 108, 2448-2456.

Bidhendi, A.J., and Geitmann, A. (2019). Methods to quantify primary plant cell wall mechanics. J Exp Bot *70*, 3615-3648.

Carbonell, A., Takeda, A., Fahlgren, N., Johnson, S.C., Cuperus, J.T., and Carrington, J.C. (2014). New generation of artificial MicroRNA and synthetic trans-acting small

1033 interfering RNA vectors for efficient gene silencing in Arabidopsis. Plant Physiol *165*,
1034 15-29.
1035 Carter, R., Woolfenden, H., Baillie, A., Amsbury, S., Carroll, S., Healicon, E.,
1036 Sovatzoglou, S., Braybrook, S., Gray, J.E., Hobbs, J.*, et al.* (2017). Stomatal Opening
1037 Involves Polar, Not Radial, Stiffening Of Guard Cells. Curr Biol *27*, 2974-2983 e2972.
1038 Cosgrove, D.J. (1993). Wall extensibility: its nature, measurement and relationship to
1039 plant cell growth. New Phytologist 124, 1-23.
1040 Cosgrove, D.J. (2016). Plant cell wall extensibility: connecting plant cell growth with cell
1041 wall structure, mechanics, and the action of wall-modifying enzymes. J Exp Bot *67*, 463-
1042 476.
1043 Cosgrove, D.J. (2018). Diffuse Growth of Plant Cell Walls. Plant Physiology *176*, 16-27.
1044 Curtis, M.D., and Grossniklaus, U. (2003). A gateway cloning vector set for high-
1045 throughput functional analysis of genes in planta. Plant Physiol *133*, 462-469.
1046 Daher, F.B., Chen, Y., Bozorg, B., Clough, J., Jönsson, H., and Braybrook, S.A. (2018).
1047 Anisotropic growth is achieved through the additive mechanical effect of material
1048 anisotropy and elastic asymmetry. Elife *7*, e38161.
1049 DeMichele, D.W., and Sharpe, P.J.H. (1973). An analysis of the mechanics of guard cell
1050 motion. Journal of Theoretical Biology *41*, 77-96.
1051 Feng, W., Kita, D., Peaucelle, A., Cartwright, H.N., Doan, V., Duan, Q., Liu, M.C.,
1052 Maman, J., Steinhorst, L., Schmitz-Thom, I.*, et al.* (2018). The FERONIA Receptor
1053 Kinase Maintains Cell-Wall Integrity during Salt Stress through Ca(2+) Signaling. Curr
1054 Biol *28*, 666-675 e665.
1055 Milani, P., Mirabet, V., Cellier, C., Rozier, F., Hamant, O., Das, P., and Boudaoud, A.
1056 (2014). Matching patterns of gene expression to mechanical stiffness at cell resolution
1057 through quantitative tandem epifluorescence and nanoindentation. Plant Physiology 165,
1058 1399-1408.
1059 Forouzesh, E., Goel, A., Mackenzie, S.A., and Turner, J.A. (2013). In vivoextraction of
1060 Arabidopsis cell turgor pressure using nanoindentation in conjunction with finite element
1061 modeling. The Plant Journal *73*, 509-520.

1062 Franks, P., Cowan, I., Tyerman, S., Cleary, A., Lloyd, J., and Farquhar, G. (1995).
1063 Guard cell pressure/aperture characteristics measured with the pressure probe. Plant,
1064 Cell & Environment *18*, 795-800.
1065 Franks, P.J., Cowan, 2 I. R., and Farquhar, G.D. (1998). A study of stomatal mechanics
1066 using the cell pressure probe. Plant, Cell & Environment *21*, 94-100.
1067 Hachez, C., Ohashi-Ito, K., Dong, J., and Bergmann, D.C. (2011). Differentiation of
1068 Arabidopsis guard cells: analysis of the networks incorporating the basic helix-loop-helix
1069 transcription factor, FAMA. Plant Physiol *155*, 1458-1472.
1070 Huang, Y.C., Wu, H.C., Wang, Y.D., Liu, C.H., Lin, C.C., Luo, D.L., and Jinn, T.L.
1071 (2017). PECTIN METHYLESTERASE34 Contributes to Heat Tolerance through Its Role
1072 in Promoting Stomatal Movement. Plant Physiol *174*, 748-763.
1073 Jezek, M., and Blatt, M.R. (2017). The Membrane Transport System of the Guard Cell
1074 and Its Integration for Stomatal Dynamics. Plant physiology *174*, 487-519.
1075 Jones, L., Milne, J.L., Ashford, D., McCann, M.C., and McQueen-Mason, S.J. (2005). A
1076 conserved functional role of pectic polymers in stomatal guard cells from a range of
1077 plant species. Planta *221*, 255-264.
1078 Jones, L., Milne, J.L., Ashford, D., and McQueen-Mason, S.J. (2003). Cell wall arabinan
1079 is essential for guard cell function. Proceedings of the National Academy of Sciences
1080 *100*, 11783-11788.
1081 Kierzkowski, D., Nakayama, N., Routier-Kierzkowska, A.-L., Weber, A., Bayer, E.,
1082 Schorderet, M., Reinhardt, D., Kuhlemeier, C., and Smith, R.S. (2012). Elastic domains
1083 regulate growth and organogenesis in the plant shoot apical meristem. Science 335,
1084 1096-1099.
1085 Kohorn, B.D., Johansen, S., Shishido, A., Todorova, T., Martinez, R., Defeo, E., and
1086 Obregon, P. (2009). Pectin activation of MAP kinase and gene expression is WAK2
1087 dependent. The Plant Journal *60*, 974-982.
1088 Lee, S., Choi, H., Suh, S., Doo, I.-S., Oh, K.-Y., Choi, E.J., Taylor, A.T.S., Low, P.S.,
1089 and Lee, Y. (1999). Oligogalacturonic acid and chitosan reduce stomatal aperture by
1090 inducing the evolution of reactive oxygen species from guard cells of tomato and
1091 Commelina communis. Plant physiology *121*, 147-152.

Leng, Y., Yang, Y., Ren, D., Huang, L., Dai, L., Wang, Y., Chen, L., Tu, Z., Gao, Y., Li, X.*, et al.* (2017). A Rice PECTATE LYASE-LIKE Gene Is Required for Plant Growth and Leaf Senescence. Plant Physiol *174*, 1151-1166.

Liners, F., Letesson, J., Didembourg, C., and Cutsem, P.V. (1989). Monoclonal antibodies against pectins: recognition of a conforma- tion induced by calcium. Plant Physiol *91*, 1419–1424.

Lionetti, V. (2015). PECTOPLATE: the simultaneous phenotyping of pectin methylesterases, pectinases, and oligogalacturonides in plants during biotic stresses. Front Plant Sci *6*, 331.

Ma, X., Zhang, X., Yang, L., Tang, M., Wang, K., Wang, L., Bai, L., and Song, C. (2019). Hydrogen peroxide plays an important role in PERK4-mediated abscisic acid-regulated root growth in Arabidopsis. Functional plant biology *46*, 165-174.

Marom, Z., Shtein, I., and Bar-On, B. (2017). Stomatal Opening: The Role of Cell-Wall Mechanical Anisotropy and Its Analytical Relations to the Bio-composite Characteristics. Front Plant Sci *8*, 2061.

McCarthy, T.W., Der, J.P., Honaas, L.A., dePamphilis, C.W., and Anderson, C.T. (2014). Phylogenetic analysis of pectin-related gene families in Physcomitrella patensand nine other plant species yields evolutionary insights into cell walls. BMC Plant Biology *14*, 79.

Meckel, T., Gall, L., Semrau, S., Homann, U., and Thiel, G. (2007). Guard cells elongate: relationship of volume and surface area during stomatal movement. Biophysical journal *92*, 1072-1080.

Mosca, G., Sapala, A., Strauss, S., Routier-Kierzkowska, A.-L., and Smith, R.S. (2017). On the micro-indentation of plant cells in a tissue context. Physical biology *14*, 015003.

Mravec, J., Kracun, S.K., Rydahl, M.G., Westereng, B., Miart, F., Clausen, M.H., Fangel, J.U., Daugaard, M., Van Cutsem, P., De Fine Licht, H.H.*, et al.* (2014). Tracking developmentally regulated post-synthetic processing of homogalacturonan and chitin using reciprocal oligosaccharide probes. Development *141*, 4841-4850.

Ohashi-Ito, K., and Bergmann, D.C. (2006). Arabidopsis FAMA Controls the Final Proliferation/Differentiation Switch during Stomatal Development. The Plant Cell *18*, 2493-2505.

1122 Ortega, J.K. (1985). Augmented growth equation for cell wall expansion. Plant
1123 physiology *79*, 318-320.
1124 Palusa, S.G., Golovkin, M., Shin, S.B., Richardson, D.N., and Reddy, A.S. (2007).
1125 Organ-specific, developmental, hormonal and stress regulation of expression of putative
1126 pectate lyase genes in Arabidopsis. New phytologist *174*, 537-550.
1127 Peaucelle, A., Braybrook, S.A., Le Guillou, L., Bron, E., Kuhlemeier, C., and Hofte, H.
1128 (2011). Pectin-induced changes in cell wall mechanics underlie organ initiation in
1129 Arabidopsis. Curr Biol *21*, 1720-1726.
1130 Powell, D., Morris, E., Gidley, M., and Rees, D. (1982). Conformations and interactions
1131 of pectins: II. Influence of residue sequence on chain association in calcium pectate
1132 gels. Journal of molecular biology *155*, 517-531.
1133 Ringli, C. (2010). Monitoring the outside: cell wall-sensing mechanisms. Plant
1134 physiology *153*, 1445-1452.
1135 Rounds, C.M., Lubeck, E., Hepler, P.K., and Winship, L.J. (2011). Propidium iodide
1136 competes with Ca(2+) to label pectin in pollen tubes and Arabidopsis root hairs. Plant
1137 Physiol *157*, 175-187.
1138 Routier-Kierzkowska, A.-L., Weber, A., Kochova, P., Felekis, D., Nelson, B.J.,
1139 Kuhlemeier, C., and Smith, R.S. (2012). Cellular force microscopy for in vivo
1140 measurements of plant tissue mechanics. Plant physiology *158*, 1514-1522.
1141 Rui, Y., and Anderson, C.T. (2016). Functional Analysis of Cellulose and Xyloglucan in
1142 the Walls of Stomatal Guard Cells of Arabidopsis. Plant Physiol *170*, 1398-1419.
1143 Rui, Y., Xiao, C., Yi, H., Kandemir, B., Wang, J.Z., Puri, V.M., and Anderson, C.T.
1144 (2017). POLYGALACTURONASE INVOLVED IN EXPANSION3 Functions in Seedling
1145 Development, Rosette Growth, and Stomatal Dynamics in Arabidopsis thaliana. Plant
1146 Cell *29*, 2413-2432.
1147 Scavetta, R.D., Herron, S.R., Hotchkiss, A.T., Kita, N., Keen, N.T., Benen, J.A., Kester,
1148 H.C., Visser, J., and Jurnak, F. (1999). Structure of a plant cell wall fragment complexed
1149 to pectate lyase C. The Plant Cell *11*, 1081-1092.
1150 Silva-Sanzana, C., Celiz-Balboa, J., Garzo, E., Marcus, S.E., Parra-Rojas, J.P., Rojas,
1151 B., Olmedo, P., Rubilar, M.A., Rios, I., and Chorbadjian, R.A. (2019). Pectin

1152 methylesterases modulate plant homogalacturonan status in defenses against the aphid
1153 Myzus persicae. The Plant Cell *31*, 1913-1929.
1154 Ström, A., Ribelles, P., Lundin, L., Norton, I., Morris, E.R., and Williams, M.A. (2007).
1155 Influence of pectin fine structure on the mechanical properties of calcium− pectin and
1156 acid− pectin gels. Biomacromolecules *8*, 2668-2674.
1157 Sun, L., and van Nocker, S. (2010). Analysis of promoter activity of members of the
1158 PECTATE LYASE-LIKE (PLL) gene family in cell separation in Arabidopsis. BMC Plant
1159 Biology *10*, 152.
1160 Verhertbruggen, Y., Marcus, S.E., Haeger, A., Ordaz-Ortiz, J.J., and Knox, J.P. (2009).
1161 An extended set of monoclonal antibodies to pectic homogalacturonan. Carbohydrate
1162 Research *344*, 1858-1862.
1163 Vogel, J.P. (2002). PMR6, a Pectate Lyase-Like Gene Required for Powdery Mildew
1164 Susceptibility in Arabidopsis. The Plant Cell Online *14*, 2095-2106.
1165 Li, W., Keynia, S., Belteton, S.A., Afshar-Hatam, F., Szymanski, D.B., and Turner, J.A.
1166 (2021). Protocol for mapping the spatial variability in cell wall mechanical bending
1167 behavior in living leaf pavement cells. bioRxiv, 2021.2002.2023.432478.
1168 Weber, A., Braybrook, S., Huflejt, M., Mosca, G., Routier-Kierzkowska, A.-L., and Smith,
1169 R.S. (2015). Measuring the mechanical properties of plant cells by combining micro-
1170 indentation with osmotic treatments. Journal of experimental botany *66*, 3229-3241.
1171 Willmer, C., and Beattie, L.N. (1978). Cellular osmotic phenomena during stomatal
1172 movements ofCommelina communis. Protoplasma 95, 321-332.
1173 Woolfenden, H.C., Bourdais, G., Kopischke, M., Miedes, E., Molina, A., Robatzek, S.,
1174 and Morris, R.J. (2017). A computational approach for inferring the cell wall properties
1175 that govern guard cell dynamics. Plant J *92*, 5-18.
1176 Wu, H.I., and Sharpe, P.J. (1979). Stomatal mechanics II*: material properties of guard
1177 cell walls. Plant, Cell & Environment *2*, 235-244.
1178 Xiao, C., Somerville, C., and Anderson, C.T. (2014). POLYGALACTURONASE
1179 INVOLVED IN EXPANSION1 functions in cell elongation and flower development in
1180 Arabidopsis. Plant Cell *26*, 1018-1035.

1181 Yakubov, G.E., Bonilla, M.R., Chen, H., Doblin, M.S., Bacic, A., Gidley, M.J., and
1182 Stokes, J.R. (2016). Mapping nano-scale mechanical heterogeneity of primary plant cell
1183 walls. Journal of experimental botany 67, 2799-2816.
1184 Yang, Y., Costa, A., Leonhardt, N., Siegel, R.S., and Schroeder, J.I. (2008). Isolation of
1185 a strong Arabidopsis guard cell promoter and its potential as a research tool. Plant
1186 Methods *4*, 6.
1187 Yi, H., Rui, Y., Kandemir, B., Wang, J.Z., Anderson, C.T., and Puri, V.M. (2018).
1188 Mechanical effects of cellulose, xyloglucan, and pectins on stomatal guard cells of
1189 Arabidopsis thaliana. Frontiers in plant science *9*, 1566.
1190 Yoder, M.D., and Jurnak, F. (1995). The refined three-dimensional structure of pectate
1191 lyase C from Erwinia chrysanthemi at 2.2 angstrom resolution (implications for an
1192 enzymatic mechanism). Plant Physiology *107*, 349-364.
1193 Zhang, X.-Q., Wei, P.-C., Xiong, Y.-M., Yang, Y., Chen, J., and Wang, X.-C. (2011).
1194 Overexpression of the Arabidopsis α-expansin gene AtEXPA1 accelerates stomatal
1195 opening by decreasing the volumetric elastic modulus. Plant cell reports *30*, 27-36.

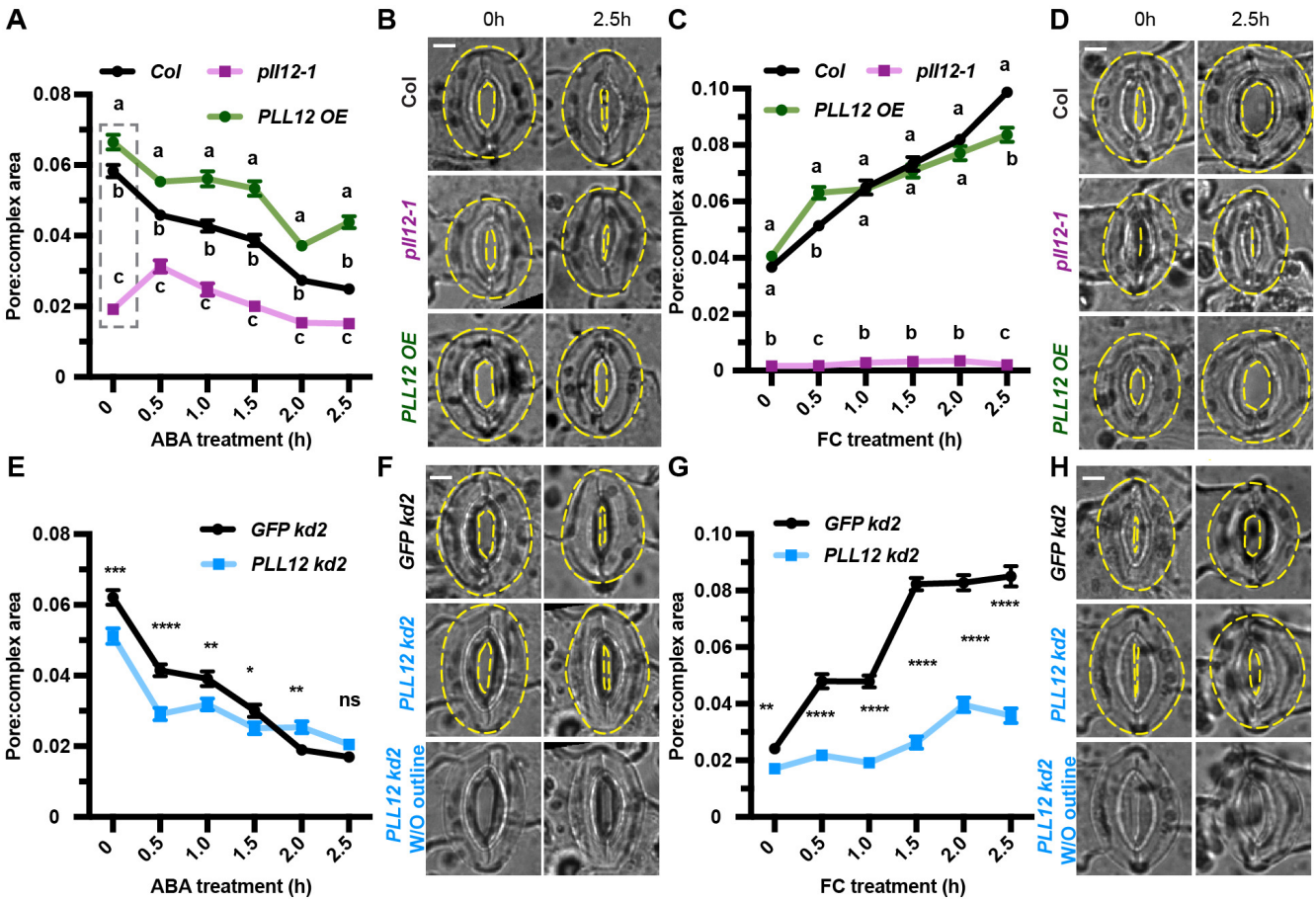

Figure 1. Expression of *PLL12* Affects Stomatal Function.
(A) Stomatal responses to 50 µM ABA in Col (black), *pll12-1 (magenta)* and *PLL12OE* (green) genotypes. Error bars indicate SEM; n ≥ 121 stomata per genotype per time point from three independent experiments. Different letters at each timepoint indicate $P < 0.05$ across genotypes for that timepoint, one-way ANOVA analysis and Tukey test (dashed gray box indicates statistical comparison group). (B) Representative images of stomata in Col*, pll12-1* and *PLL12OE* plants before and after 2.5 h ABA treatment. Stomatal complexes and pores are outlined by yellow dashed lines. Bar = 5 µm. (C-D) as in (A-B) but treated with 1 µM FC and n ≥ 122 stomata per genotype per timepoint. Bar = 5 µm. (E) Comparison of stomatal responses to 50 µM ABA between GFP kd-2 (black) and PLL12 kd-2 (blue) plants. Error bars indicate SEM; asterisks indicate significant difference between genotypes at each time point examined: **** $P < 0.0001$, Student's t-test; n ≥ 102 stomata per genotype per time point from three independent experiments and six biological replicates in total. (F) As in (B) but for GFP kd-2 and PLL12 kd-2. Images without outlines of PLL12 kd2 are also shown. Bar = 5 µm. (G-H) As in (E-F) but treated with 1 µM FC and n ≥ 112 stomata. Bar = 5 µm.

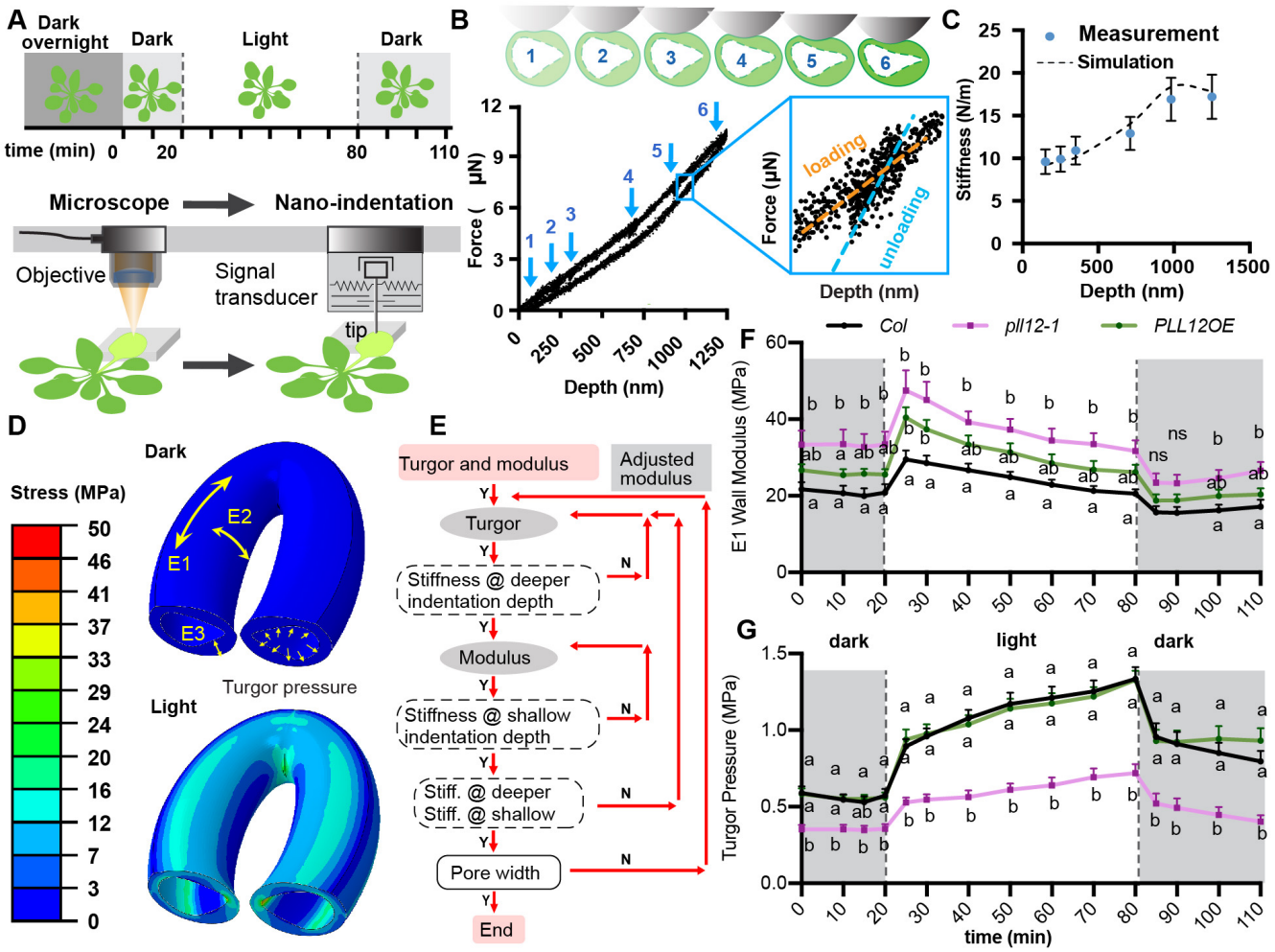

Figure 2. Altered *PLL12* Expression Affects Turgor Pressure More Than Wall Modulus in Guard Cells.

(A) Illustration of stiffness measurements by nanoindentation and experimental set up. Plants were kept in the dark overnight to ensure stomatal closure, and nanoindentation was performed at least every 10 min during the experiment. At 20 min after the first measurement (T0), light was turned on for 60 min to induce stomatal opening, then the light was turned off and measurements were collected for 30 min. The abaxial side of leaf seven was gently twisted to face upward, a target guard cell was located under the microscope, then the nanoindentation probe (tip radius = 2~3 μm) was moved to the same location. At each time point, stiffness in the same guard cell was measured at six different depths (B). (B) Diagram of indentation at different depths, representative force - depth curve for one guard cell, and definition of stiffness. Loading - unloading curves of all six different depths are shown by blue numbers. A zoomed in view of a loading (orange) and unloading (blue) curve at the fifth depth is shown in the blue box. Stiffness is defined as the slope of the unloading curve. (C) Simulation of calculated stiffness to six different depths. Blue dots represent the calculated stiffness from nanoindentation measurements; dashed line represents the results of the simulation. Bars = SD. (D) Representative FEM models. Upper and lower images represent modeled guard cell shapes before (dark) and after pressurization (light), respectively. Longitudinal modulus E1 was set to be the same as radial modulus E3, and both are four times smaller than circumferential modulus E2. (E) Illustration of iteration process to derive turgor pressure and wall modulus from nanoindentation simulation and FEM. (F-G) Wall modulus (F) and turgor pressure (G) derived for each genotype. n = 9 guard cells from at least five plants per genotype. Different letters at each timepoint indicate $P < 0.05$ across genotypes for that timepoint, two-way ANOVA analysis and Tukey test. Bars = SEM; ns = no significant difference.

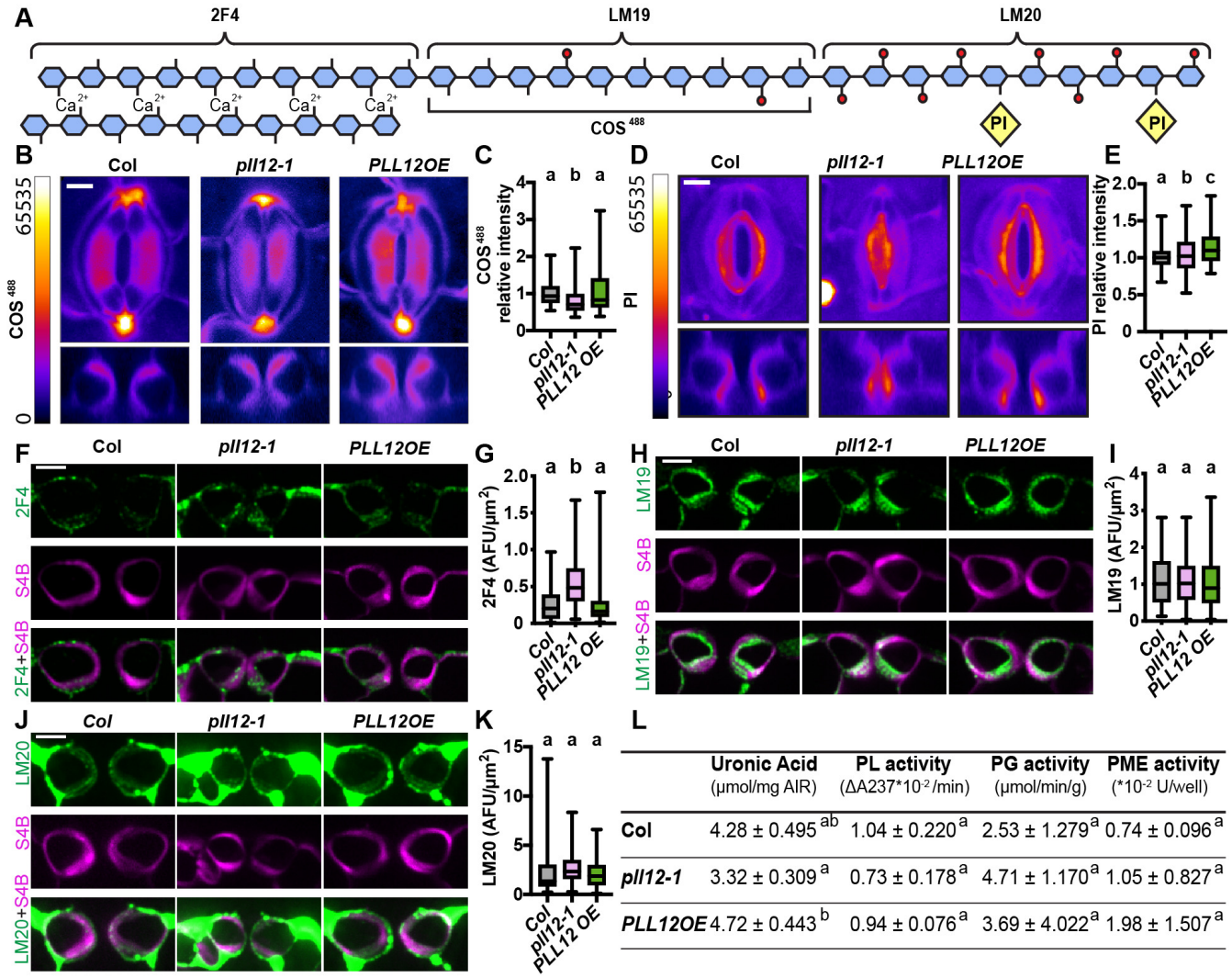

L

	Uronic Acid (µmol/mg AIR)	PL activity (ΔA237*10^{-2}/min)	PG activity (µmol/min/g)	PME activity (*10^{-2} U/well)
Col	4.28 ± 0.495 ^{ab}	1.04 ± 0.220 ^{a}	2.53 ± 1.279 ^{a}	0.74 ± 0.096 ^{a}
pll12-1	3.32 ± 0.309 ^{a}	0.73 ± 0.178 ^{a}	4.71 ± 1.170 ^{a}	1.05 ± 0.827 ^{a}
PLL12OE	4.72 ± 0.443 ^{b}	0.94 ± 0.076 ^{a}	3.69 ± 4.022 ^{a}	1.98 ± 1.507 ^{a}

Figure 3. *PLL12* Influences HG Labeling in Guard Cell Walls.

(A) Diagram showing different epitopes of HG that are recognized by the dyes and antibodies. Blue pentagon represents GalA, with or without red circle on Gal represents methylated or unmethylated GalA. Yellow square represents PI molecule. (B) Representative XY (upper panel) and XZ (lower panel) maximum projection images of COS488 labeling. Images are displayed with a fire look-up table, XZ projections were made from the midline in the Y direction. Bar = 5 µm. (C) Quantification of relative intensity of COS488 labeling in guard cells from 3- to 4-week-old Col, *pll12-1* and *PLL12 OE* plants. Whiskers extend to min and max, box boundaries indicate first and third quartiles of datasets, and horizontal lines inside boxes represent medians; n ≥ 153 guard cells per genotype from two independent experiments, six plants in total. Different letters indicate $P < 0.05$, one-way ANOVA and Tukey test. (D-E) as in (B-C) but stained with Propidium Iodide (PI) and n ≥ 131 guard cells per genotype. (F) Representative images of cross sections of guard cells from Col, *pll12-1* and *PLL12 OE* plants, immunolabeled with 2F4 (green) and counterstained with S4B (magenta). Bars = 5 µm. (G) Quantification of 2F4 labeling intensity in cross-sections of guard cells from 3- to 4-week-old Col, *pll12-1* and *PLL12 OE* plants. Error bars indicate SEM; n ≥ 112 guard cells per genotype from at least two independent experiments, three different leaves. Different letters indicate $P < 0.05$, or no significant differences across genotypes, one-way ANOVA and Tukey test. (H-K) as in (F-G) but labeled with LM19 (H-I) or LM20 (J-K). (L) Uronic acid content, and PL (pectate lyase), PG (polygalacturonase) and PME (pectin methylesterase) enzymatic activity in Col, *pll12-1*, and *PLL12 OE* rosettes. For uronic acid content, PG, and PME assays n = three independent experiments each with five technical replicates per genotype. For the PL assay, n = three independent experiments each with three technical replicates per genotype. Values are mean ± SD. Different letters indicate $P < 0.05$, one-way ANOVA and Tukey test.

Figure 4

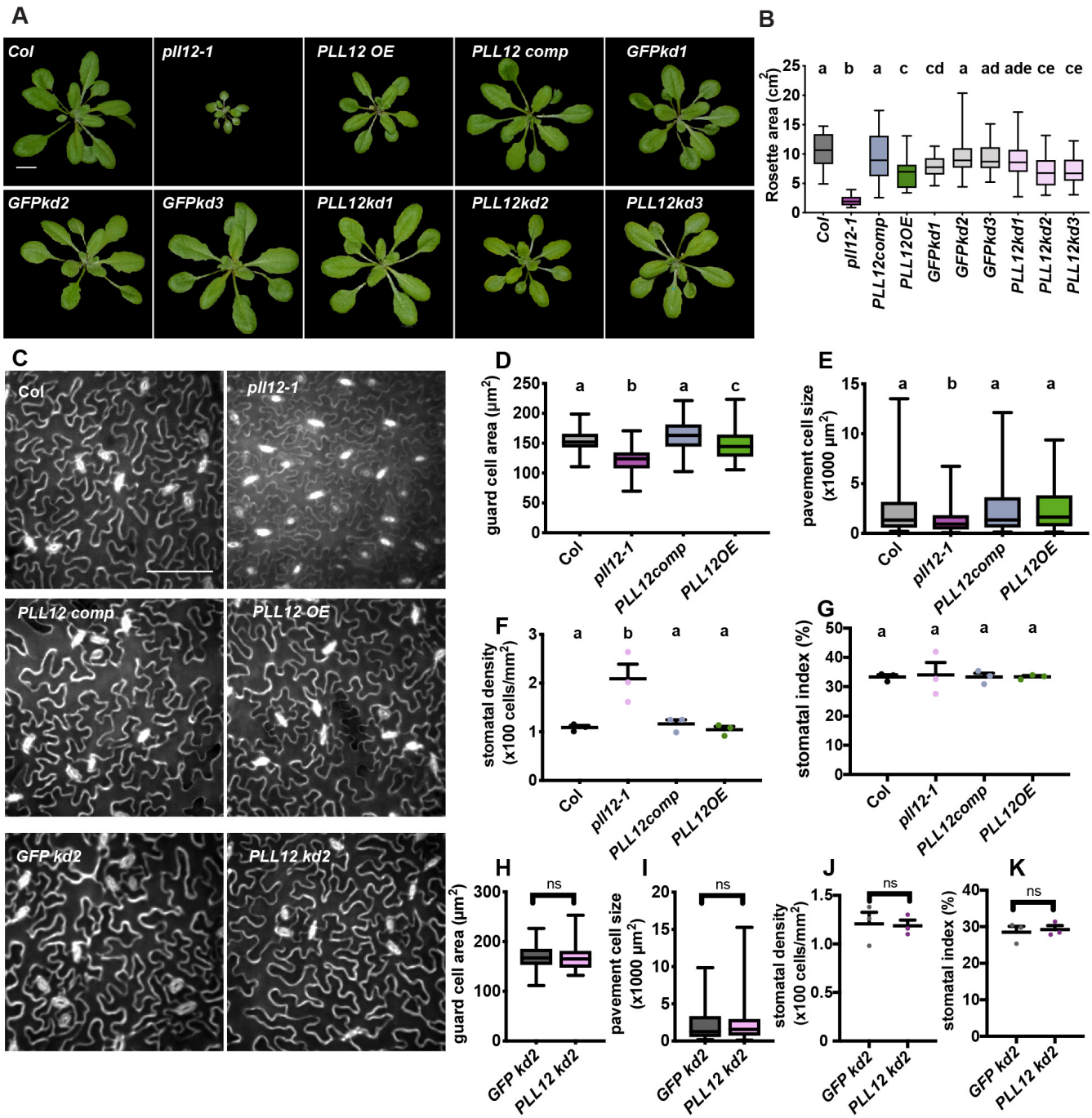
A
Col
pll12-1
PLL12 OE
PLL12 comp
GFPkd1
GFPkd2
GFPkd3
PLL12kd1
PLL12kd2
PLL12kd3
B
Rosette area (cm²)
a b a c cd a ad ade ce ce
Col
pll12-1
PLL12comp
PLL12OE
GFPkd1
GFPkd2
GFPkd3
PLL12kd1
PLL12kd2
PLL12kd3
C
Col
pll12-1
PLL12 comp
PLL12 OE
GFP kd2
PLL12 kd2
D
guard cell area (µm²)
a b a c
E
pavement cell size (x1000 µm²)
a b a a
F
stomatal density (x100 cells/mm²)
a b a a
G
stomatal index (%)
a a a a
H
guard cell area (µm²)
ns
I
pavement cell size (x1000 µm²)
ns
J
stomatal density (x100 cells/mm²)
ns
K
stomatal index (%)
ns
GFP kd2
PLL12 kd2

Figure 4. *PLL12* Expression Affects Plant Growth, Epidermal Cell Expansion and Proliferation.

(A) Representative rosette images of 21-d-old Col, *pll12-1*, *PLL12* overexpression (*PLL12 OE*), *PLL12* complementation (*PLL12 comp*) and guard cell-specific knockdown pGC1::GFP kd-1 to -3 and pGC1::PLL12 kd-1 to -3 lines. Bar = 1 cm. (B) Rosette areas of 21-d-old Col and *PLL12* transgenic plants; n≥35 plants per genotype from three independent experiments. (C) Representative images of epidermal cells stained with Propidium Iodide in 21-d-old *Col, pll12-1, PLL12 OE, PLL12 comp, GFP kd-2* and *PLL12 kd-2* plants. Enhance contrast was performed on the maximum projection of z-stack images. Bar = 100 µm. (D-G) Quantification of guard cell area (D), pavement cell size (E), stomatal density (F) and stomatal index (G) in 21-d-old Col*, pll12-1, PLL12 OE, PLL12 comp* plants. n ≥ 74 (D) and n ≥ 99 (H) guard cells from three individual plants per genotype. n ≥ 223 (E) and n ≥ 105 (I) pavement cells from at least three individual plants per genotype. n = three individual plants (F-G and J-K) with five fields of each were imaged and quantified for density and index analysis. Stomatal index = number of stomata (n_s) divided by the sum of stomata number and pavement cell number (n_p) per field ($n_s/(n_s+n_p)$). Different letters denote $P < 0.05$, one-way ANOVA and Tukey test. (F-I) as in (B-E) but for *GFP kd-2* and *PLL12 kd-2* plants. Dark gray dots or box represent Col, magenta for *pll12-1*, blue for *PLL12comp*, green for *PLL12OE*, light gray for *GFPkd*, and pink for *PLL12kd*. Error bars indicate SD. Whiskers extend to min and max, box boundaries indicate first and third quartiles of datasets, and horizontal lines inside boxes represent medians.

Parsed Citations

Amsbury, S., Hunt, L., Elhaddad, N., Baillie, A., Lundgren, M., Verhertbruggen, Y., Scheller, H.V., Knox, J.P., Fleming, A.J., and Gray, J.E. (2016). Stomatal Function Requires Pectin De-methyl-esterification of the Guard Cell Wall. Curr Biol 26, 2899-2906.
Google Scholar: Author Only Title Only Author and Title

Anderson, C.T. (2016). We be jammin': an update on pectin biosynthesis, trafficking and dynamics. J Exp Bot 67, 495-502.
Google Scholar: Author Only Title Only Author and Title

Aylor, D.E., Parlange, J.-Y., and Krikorian, A.D. (1973). STOMATAL MECHANICS. American Journal of Botany 60, 163-171.
Google Scholar: Author Only Title Only Author and Title

Babu, Y., and Bayer, M. (2014). Plant Polygalacturonases involved in cell elongation and separation-the same but different? Plants 3, 613-623.
Google Scholar: Author Only Title Only Author and Title

Bai, L., Zhang, G., Zhou, Y., Zhang, Z., Wang, W., Du, Y., Wu, Z., and Song, C.P. (2009). Plasma membrane-associated proline-rich extensin-like receptor kinase 4, a novel regulator of Ca2+ signalling, is required for abscisic acid responses in Arabidopsis thaliana. The Plant Journal 60, 314-327.
Google Scholar: Author Only Title Only Author and Title

Beauzamy, L., Derr, J., and Boudaoud, A. (2015). Quantifying hydrostatic pressure in plant cells by using indentation with an atomic force microscope. Biophysical journal 108, 2448-2456.
Google Scholar: Author Only Title Only Author and Title

Bidhendi, A.J., and Geitmann, A. (2019). Methods to quantify primary plant cell wall mechanics. J Exp Bot 70, 3615-3648.
Google Scholar: Author Only Title Only Author and Title

Carbonell, A., Takeda, A., Fahlgren, N., Johnson, S.C., Cuperus, J.T., and Carrington, J.C. (2014). New generation of artificial MicroRNA and synthetic trans-acting small interfering RNA vectors for efficient gene silencing in Arabidopsis. Plant Physiol 165, 15-29.
Google Scholar: Author Only Title Only Author and Title

Carter, R., Woolfenden, H., Baillie, A., Amsbury, S., Carroll, S., Healicon, E., Sovatzoglou, S., Braybrook, S., Gray, J.E., Hobbs, J., et al. (2017). Stomatal Opening Involves Polar, Not Radial, Stiffening Of Guard Cells. Curr Biol 27, 2974-2983 e2972.
Google Scholar: Author Only Title Only Author and Title

Cosgrove, D.J. (1993). Wall extensibility: its nature, measurement and relationship to plant cell growth. New Phytologist 124, 1-23.
Google Scholar: Author Only Title Only Author and Title

Cosgrove, D.J. (2016). Plant cell wall extensibility: connecting plant cell growth with cell wall structure, mechanics, and the action of wall-modifying enzymes. J Exp Bot 67, 463-476.
Google Scholar: Author Only Title Only Author and Title

Cosgrove, D.J. (2018). Diffuse Growth of Plant Cell Walls. Plant Physiology 176, 16-27.
Google Scholar: Author Only Title Only Author and Title

Curtis, M.D., and Grossniklaus, U. (2003). A gateway cloning vector set for high-throughput functional analysis of genes in planta. Plant Physiol 133, 462-469.
Google Scholar: Author Only Title Only Author and Title

Daher, F.B., Chen, Y., Bozorg, B., Clough, J., Jönsson, H., and Braybrook, S.A. (2018). Anisotropic growth is achieved through the additive mechanical effect of material anisotropy and elastic asymmetry. Elife 7, e38161.
Google Scholar: Author Only Title Only Author and Title

DeMichele, D.W., and Sharpe, P.J.H. (1973). An analysis of the mechanics of guard cell motion. Journal of Theoretical Biology 41, 77-96.
Google Scholar: Author Only Title Only Author and Title

Feng, W., Kita, D., Peaucelle, A., Cartwright, H.N., Doan, V., Duan, Q., Liu, M.C., Maman, J., Steinhorst, L., Schmitz-Thom, I., et al. (2018). The FERONIA Receptor Kinase Maintains Cell-Wall Integrity during Salt Stress through Ca(2+) Signaling. Curr Biol 28, 666-675 e665.
Google Scholar: Author Only Title Only Author and Title

Milani, P., Mirabet, V., Cellier, C., Rozier, F., Hamant, O., Das, P., and Boudaoud, A. (2014). Matching patterns of gene expression to mechanical stiffness at cell resolution through quantitative tandem epifluorescence and nanoindentation. Plant Physiology 165, 1399-1408.
Google Scholar: Author Only Title Only Author and Title

Forouzesh, E., Goel, A., Mackenzie, S.A., and Turner, J.A. (2013). In vivoextraction of Arabidopsis cell turgor pressure using nanoindentation in conjunction with finite element modeling. The Plant Journal 73, 509-520.
Google Scholar: Author Only Title Only Author and Title

Franks, P., Cowan, I., Tyerman, S., Cleary, A., Lloyd, J., and Farquhar, G. (1995). Guard cell pressure/aperture characteristics measured with the pressure probe. Plant, Cell & Environment 18, 795-800.
Google Scholar: Author Only Title Only Author and Title

Franks, P.J., Cowan, 2 I. R., and Farquhar, G.D. (1998). A study of stomatal mechanics using the cell pressure probe. Plant, Cell & Environment 21, 94-100.
Google Scholar: Author Only Title Only Author and Title

Hachez, C., Ohashi-Ito, K., Dong, J., and Bergmann, D.C. (2011). Differentiation of Arabidopsis guard cells: analysis of the networks incorporating the basic helix-loop-helix transcription factor, FAMA. Plant Physiol 155, 1458-1472.
Google Scholar: Author Only Title Only Author and Title

Huang, Y.C., Wu, H.C., Wang, Y.D., Liu, C.H., Lin, C.C., Luo, D.L., and Jinn, T.L. (2017). PECTIN METHYLESTERASE34 Contributes to Heat Tolerance through Its Role in Promoting Stomatal Movement. Plant Physiol 174, 748-763.
Google Scholar: Author Only Title Only Author and Title

Jezek, M., and Blatt, M.R. (2017). The Membrane Transport System of the Guard Cell and Its Integration for Stomatal Dynamics. Plant physiology 174, 487-519.
Google Scholar: Author Only Title Only Author and Title

Jones, L., Milne, J.L., Ashford, D., McCann, M.C., and McQueen-Mason, S.J. (2005). A conserved functional role of pectic polymers in stomatal guard cells from a range of plant species. Planta 221, 255-264.
Google Scholar: Author Only Title Only Author and Title

Jones, L., Milne, J.L., Ashford, D., and McQueen-Mason, S.J. (2003). Cell wall arabinan is essential for guard cell function. Proceedings of the National Academy of Sciences 100, 11783-11788.
Google Scholar: Author Only Title Only Author and Title

Kierzkowski, D., Nakayama, N., Routier-Kierzkowska, A.-L., Weber, A., Bayer, E., Schorderet, M., Reinhardt, D., Kuhlemeier, C., and Smith, R.S. (2012). Elastic domains regulate growth and organogenesis in the plant shoot apical meristem. Science 335, 1096-1099.
Google Scholar: Author Only Title Only Author and Title

Kohorn, B.D., Johansen, S., Shishido, A, Todorova, T., Martinez, R., Defeo, E., and Obregon, P. (2009). Pectin activation of MAP kinase and gene expression is WAK2 dependent. The Plant Journal 60, 974-982.
Google Scholar: Author Only Title Only Author and Title

Lee, S., Choi, H., Suh, S., Doo, I.-S., Oh, K.-Y., Choi, E.J., Taylor, A.T.S., Low, P.S., and Lee, Y. (1999). Oligogalacturonic acid and chitosan reduce stomatal aperture by inducing the evolution of reactive oxygen species from guard cells of tomato and Commelina communis. Plant physiology 121, 147-152.
Google Scholar: Author Only Title Only Author and Title

Leng, Y., Yang, Y., Ren, D., Huang, L., Dai, L., Wang, Y., Chen, L., Tu, Z., Gao, Y., Li, X., et al. (2017). A Rice PECTATE LYASE-LIKE Gene Is Required for Plant Growth and Leaf Senescence. Plant Physiol 174, 1151-1166.
Google Scholar: Author Only Title Only Author and Title

Liners, F., Letesson, J., Didembourg, C., and Cutsem, P.V. (1989). Monoclonal antibodies against pectins: recognition of a conformation induced by calcium. Plant Physiol 91, 1419–1424.
Google Scholar: Author Only Title Only Author and Title

Lionetti, V. (2015). PECTOPLATE: the simultaneous phenotyping of pectin methylesterases, pectinases, and oligogalacturonides in plants during biotic stresses. Front Plant Sci 6, 331.
Google Scholar: Author Only Title Only Author and Title

Ma, X., Zhang, X., Yang, L., Tang, M., Wang, K., Wang, L., Bai, L., and Song, C. (2019). Hydrogen peroxide plays an important role in PERK4-mediated abscisic acid-regulated root growth in Arabidopsis. Functional plant biology 46, 165-174.
Google Scholar: Author Only Title Only Author and Title

Marom, Z., Shtein, I., and Bar-On, B. (2017). Stomatal Opening: The Role of Cell-Wall Mechanical Anisotropy and Its Analytical Relations to the Bio-composite Characteristics. Front Plant Sci 8, 2061.
Google Scholar: Author Only Title Only Author and Title

McCarthy, T.W., Der, J.P., Honaas, L.A., dePamphilis, C.W., and Anderson, C.T. (2014). Phylogenetic analysis of pectin-related gene families in Physcomitrella patensand nine other plant species yields evolutionary insights into cell walls. BMC Plant Biology 14, 79.
Google Scholar: Author Only Title Only Author and Title

Meckel, T., Gall, L., Semrau, S., Homann, U., and Thiel, G. (2007). Guard cells elongate: relationship of volume and surface area during stomatal movement. Biophysical journal 92, 1072-1080.
Google Scholar: Author Only Title Only Author and Title

Mosca, G., Sapala, A., Strauss, S., Routier-Kierzkowska, A.-L., and Smith, R.S. (2017). On the micro-indentation of plant cells in a tissue context. Physical biology 14, 015003.
Google Scholar: Author Only Title Only Author and Title

Mravec, J., Kracun, S.K., Rydahl, M.G., Westereng, B., Miart, F., Clausen, M.H., Fangel, J.U., Daugaard, M., Van Cutsem, P., De Fine Licht, H.H., et al. (2014). Tracking developmentally regulated post-synthetic processing of homogalacturonan and chitin using reciprocal oligosaccharide probes. Development 141, 4841-4850.
Google Scholar: Author Only Title Only Author and Title

Ohashi-Ito, K., and Bergmann, D.C. (2006). Arabidopsis FAMA Controls the Final Proliferation/Differentiation Switch during Stomatal Development. The Plant Cell 18, 2493-2505.
Google Scholar: Author Only Title Only Author and Title

Ortega, J.K. (1985). Augmented growth equation for cell wall expansion. Plant physiology 79, 318-320.
Google Scholar: Author Only Title Only Author and Title

Palusa, S.G., Golovkin, M., Shin, S.B., Richardson, D.N., and Reddy, A.S. (2007). Organ-specific, developmental, hormonal and stress regulation of expression of putative pectate lyase genes in Arabidopsis. New phytologist 174, 537-550.
Google Scholar: Author Only Title Only Author and Title

Peaucelle, A., Braybrook, S.A., Le Guillou, L., Bron, E., Kuhlemeier, C., and Hofte, H. (2011). Pectin-induced changes in cell wall mechanics underlie organ initiation in Arabidopsis. Curr Biol 21, 1720-1726.
Google Scholar: Author Only Title Only Author and Title

Powell, D., Morris, E., Gidley, M., and Rees, D. (1982). Conformations and interactions of pectins: II. Influence of residue sequence on chain association in calcium pectate gels. Journal of molecular biology 155, 517-531.
Google Scholar: Author Only Title Only Author and Title

Ringli, C. (2010). Monitoring the outside: cell wall-sensing mechanisms. Plant physiology 153, 1445-1452.
Google Scholar: Author Only Title Only Author and Title

Rounds, C.M., Lubeck, E., Hepler, P.K., and Winship, L.J. (2011). Propidium iodide competes with Ca(2+) to label pectin in pollen tubes and Arabidopsis root hairs. Plant Physiol 157, 175-187.
Google Scholar: Author Only Title Only Author and Title

Routier-Kierzkowska, A.-L., Weber, A., Kochova, P., Felekis, D., Nelson, B.J., Kuhlemeier, C., and Smith, R.S. (2012). Cellular force microscopy for in vivo measurements of plant tissue mechanics. Plant physiology 158, 1514-1522.
Google Scholar: Author Only Title Only Author and Title

Rui, Y., and Anderson, C.T. (2016). Functional Analysis of Cellulose and Xyloglucan in the Walls of Stomatal Guard Cells of Arabidopsis. Plant Physiol 170, 1398-1419.
Google Scholar: Author Only Title Only Author and Title

Rui, Y., Xiao, C., Yi, H., Kandemir, B., Wang, J.Z., Puri, V.M., and Anderson, C.T. (2017). POLYGALACTURONASE INVOLVED IN EXPANSION3 Functions in Seedling Development, Rosette Growth, and Stomatal Dynamics in Arabidopsis thaliana. Plant Cell 29, 2413-2432.
Google Scholar: Author Only Title Only Author and Title

Scavetta, R.D., Herron, S.R., Hotchkiss, A.T., Kita, N., Keen, N.T., Benen, J.A., Kester, H.C., Visser, J., and Jurnak, F. (1999). Structure of a plant cell wall fragment complexed to pectate lyase C. The Plant Cell 11, 1081-1092.
Google Scholar: Author Only Title Only Author and Title

Silva-Sanzana, C., Celiz-Balboa, J., Garzo, E., Marcus, S.E., Parra-Rojas, J.P., Rojas, B., Olmedo, P., Rubilar, M.A., Rios, I., and Chorbadjian, R.A. (2019). Pectin methylesterases modulate plant homogalacturonan status in defenses against the aphid Myzus persicae. The Plant Cell 31, 1913-1929.
Google Scholar: Author Only Title Only Author and Title

Ström, A., Ribelles, P., Lundin, L., Norton, I., Morris, E.R., and Williams, M.A. (2007). Influence of pectin fine structure on the mechanical properties of calcium− pectin and acid− pectin gels. Biomacromolecules 8, 2668-2674.
Google Scholar: Author Only Title Only Author and Title

Sun, L., and van Nocker, S. (2010). Analysis of promoter activity of members of the PECTATE LYASE-LIKE (PLL) gene family in cell separation in Arabidopsis. BMC Plant Biology 10, 152.
Google Scholar: Author Only Title Only Author and Title

Verhertbruggen, Y., Marcus, S.E., Haeger, A., Ordaz-Ortiz, J.J., and Knox, J.P. (2009). An extended set of monoclonal antibodies to pectic homogalacturonan. Carbohydrate Research 344, 1858-1862.
Google Scholar: Author Only Title Only Author and Title

Vogel, J.P. (2002). PMR6, a Pectate Lyase-Like Gene Required for Powdery Mildew Susceptibility in Arabidopsis. The Plant Cell Online 14, 2095-2106.
Google Scholar: Author Only Title Only Author and Title

Li, W., Keynia, S., Belteton, S.A., Afshar-Hatam, F., Szymanski, D.B., and Turner, J.A. (2021). Protocol for mapping the spatial variability in cell wall mechanical bending behavior in living leaf pavement cells. bioRxiv, 2021.2002.2023.432478.
Google Scholar: Author Only Title Only Author and Title

Weber, A., Braybrook, S., Huflejt, M., Mosca, G., Routier-Kierzkowska, A.-L., and Smith, R.S. (2015). Measuring the mechanical properties of plant cells by combining micro-indentation with osmotic treatments. Journal of experimental botany 66, 3229-3241.
Google Scholar: Author Only Title Only Author and Title

Willmer, C., and Beattie, L.N. (1978). Cellular osmotic phenomena during stomatal movements ofCommelina communis. Protoplasma 95,

321-332.
Google Scholar: Author Only Title Only Author and Title

Woolfenden, H.C., Bourdais, G., Kopischke, M., Miedes, E., Molina, A., Robatzek, S., and Morris, R.J. (2017). A computational approach for inferring the cell wall properties that govern guard cell dynamics. Plant J 92, 5-18.
Google Scholar: Author Only Title Only Author and Title

Wu, H.I., and Sharpe, P.J. (1979). Stomatal mechanics II*: material properties of guard cell walls. Plant, Cell & Environment 2, 235-244.
Google Scholar: Author Only Title Only Author and Title

Xiao, C., Somerville, C., and Anderson, C.T. (2014). POLYGALACTURONASE INVOLVED IN EXPANSION1 functions in cell elongation and flower development in Arabidopsis. Plant Cell 26, 1018-1035.
Google Scholar: Author Only Title Only Author and Title

Yakubov, G.E., Bonilla, M.R., Chen, H., Doblin, M.S., Bacic, A., Gidley, M.J., and Stokes, J.R. (2016). Mapping nano-scale mechanical heterogeneity of primary plant cell walls. Journal of experimental botany 67, 2799-2816.
Google Scholar: Author Only Title Only Author and Title

Yang, Y., Costa, A., Leonhardt, N., Siegel, R.S., and Schroeder, J.I. (2008). Isolation of a strong Arabidopsis guard cell promoter and its potential as a research tool. Plant Methods 4, 6.
Google Scholar: Author Only Title Only Author and Title

Yi, H., Rui, Y., Kandemir, B., Wang, J.Z., Anderson, C.T., and Puri, V.M. (2018). Mechanical effects of cellulose, xyloglucan, and pectins on stomatal guard cells of Arabidopsis thaliana. Frontiers in plant science 9, 1566.
Google Scholar: Author Only Title Only Author and Title

Yoder, M.D., and Jurnak, F. (1995). The refined three-dimensional structure of pectate lyase C from Erwinia chrysanthemi at 2.2 angstrom resolution (implications for an enzymatic mechanism). Plant Physiology 107, 349-364.
Google Scholar: Author Only Title Only Author and Title

Zhang, X.-Q., Wei, P.-C., Xiong, Y.-M., Yang, Y., Chen, J., and Wang, X.-C. (2011). Overexpression of the Arabidopsis α-expansin gene AtEXPA1 accelerates stomatal opening by decreasing the volumetric elastic modulus. Plant cell reports 30, 27-36.
Google Scholar: Author Only Title Only Author and Title